Molecular Pharmacology Fast Forward. Published on January 22, 2008 as doi:10.1124/mol.107.042861

Improvement of Cyclophosphamide Activation by CYP2B6 Mutants: from *in Silico* to *ex Vivo*

Thien-An Nguyen, Marina Tychopoulos, Florence Bichat, Clothilde Zimmermann, Jean-Pierre Flinois, Monique Diry, Emelie Ahlberg, Marcel Delaforge, Laurent Corcos, Philippe Beaune, Patrick Dansette, François André and Isabelle de Waziers.

CEA, iBiTecS, URA 2096 CNRS, SB2SM, Gif sur Yvette, F-91191, France. (TAN, MD, FA)

INSERM, UMR775, Paris, F-75006 France; Université Paris Descartes, Paris, F-75006 France; APHP, Hôpital Européen Georges Pompidou, Paris, F-75015, France. (MT, CZ, JPF, MD, EA, PB, IW)

INSERM, UMR517, Dijon, F-21033 France (FB)

INSERM, U613/EA948, Brest, F-29000 France (LC)

CNRS, UMR8601, Paris, F-75006 France; Université Paris Descartes, Paris, F-75006 France (PD)

Molecular Pharmacology Fast Forward. Published on January 22, 2008 as DOI: 10.1124/mol.107.042861
This article has not been copyedited and formatted. The final version may differ from this version.

Running title page

a) Running title: Improvement of cyclophosphamide activation by CYP2B6 mutants.

b) Corresponding author. Mailing address: Isabelle de Waziers, INSERM UMR-S775, Faculté de Médecine, 45 rue des Saints Pères 75270 Paris Cedex 06, France. Phone: (33) 1 42 86 21 49, Fax: (33) 1 42 86 20 72, e-mail: isabelle.waziers@univ-paris5.fr

c) Number of text pages: 31

Number of Tables: 2

Number of Figures: 9

Number of References: 40

Number of words in Abstract: 247

Number of words in Introduction: 732

Number of words in Discussion: 1492

d) **Abbreviations**: CYP, cytochrome P450; CPA, cyclophosphamide; 3D, three-dimensional; SRS, substrate recognition site; RED, NADPH cytochrome P450 reductase; 7-EC, 7-ethoxycoumarin; 7-EFC, 7-ethoxy-4-trifluoromethyl coumarin; RMSD, root mean square deviation; GDEPT, gene-directed enzyme prodrug therapy; MD, molecular dynamics; CPI, 4-(4-chlorophenyl)imidazole; SMAS, solvent molecular accessible surface; MOI, multiplicity of infection.

Molecular Pharmacology Fast Forward. Published on January 22, 2008 as DOI: 10.1124/mol.107.042861
This article has not been copyedited and formatted. The final version may differ from this version.

Abstract

Cyclophosphamide (CPA) is a chemotherapeutic agent that is primarily activated in the liver by cytochrome P4502B6 (CYP2B6) and is then transported to the tumor via blood flow. To prevent deleterious secondary effects, CYP-based gene-directed enzyme prodrug therapy (GDEPT) consists of expressing CYP2B6 in tumor cells before CPA treatment. Given the relatively low affinity of CYP2B6 for CPA, the aim of our work was to modify CYP2B6 in order to increase its catalytic efficiency (Vmax/Km) to metabolize CPA into 4'-OH CPA. A molecular model of CYP2B6 was built and four residues in close contact with the substrate were subjected to mutagenesis. Canine CYP2B11 exhibiting a particularly low Km to CPA, the amino acids exclusively present in the CYP2B11 substrate recognition sequences were substituted in human CYP2B6. All mutants (n=26) were expressed in *Saccharomyces cerevisiae* and their enzymatic constants (Km, Vmax) evaluated using CPA as substrate. Five mutants exhibited a two to three-fold higher catalytic efficiency than wt CYP2B6. A double mutant, comprising the two most effective mutations, showed a 4-fold increase in Km/Vmax. Molecular dynamic simulations of several mutants were found to be consistent with the observed modifications incatalytic efficiency. Finally, expression of the CYP2B6 114V/477W double mutant, contrary to wt CYP2B6, allowed switching of a resistant human head and neck cancer cell line (A-253) into a sensitive cell line towards CPA. Thus, we were able to obtain a new efficient CYP2B6 mutant able to metabolize CPA, an important step in the GDEPT strategy for human cancer treatment.

Molecular Pharmacology Fast Forward. Published on January 22, 2008 as DOI: 10.1124/mol.107.042861
This article has not been copyedited and formatted. The final version may differ from this version.

Introduction

Cyclophosphamide (CPA) is a widely used chemotherapeutic agent that requires activation by cytochrome P450 2B6 (CYP2B6) in order to exert its cytotoxic effects through DNA cross-links (Gervot et al., 1999; Roy et al., 1999). In patients with cancer, CPA is primarily activated in the liver and the activated metabolite is transported to the tumor via blood flow. However, these cytotoxic metabolites also gain entry to non-tumoral tissues where they may induce several side effects, including cardiotoxicity, renal toxicity, bone marrow suppression and neurotoxicity (Ayash et al., 1992; Goren et al., 1986; Peters et al., 1993). To prevent these deleterious secondary effects, CYP-based gene-directed enzyme prodrug therapy (GDEPT) has been proposed. This strategy consists of the introduction of a vector that allows for CYP2B6 expression into tumor cells before CPA treatment. It was first developed by D.J Waxman's group (Jounaidi, 2002; Waxman et al., 1999) and more recently by our laboratory (Tychopoulos et al., 2005). Due to the intra-tumoral activation of CPA, this approach increases both the sensitivity and selectivity of cancer therapy, resulting in higher efficacy and reduced host tissue toxicity (Braybrooke et al., 2005).

One of the major drawbacks of this strategy is the relatively low affinity of CYP2B6 for CPA, which shows a high Km. The aim of this work was to modify the CYP2B6 enzyme in order to increase its catalytic efficiency (Vmax/Km) for 4-hydroxylation of CPA and, therefore, to improve its therapeutic effect. The concept of creating "improved" enzymes is not new and previous structure-function studies on mammalian CYPs have shown that some mutations can enhance existing activities or confer new specificities (Chen et al., 2004; Domanski and Halpert, 2001; Melet et

Molecular Pharmacology Fast Forward. Published on January 22, 2008 as DOI: 10.1124/mol.107.042861
This article has not been copyedited and formatted. The final version may differ from this version.

al., 2003; Spatzenegger et al., 2003). In order to engineer CYP2B6 with increased catalytic efficiency for 4-OH-CPA hydroxylation, two approaches were used.

First, as there is no crystal structure of CYP2B6 available in the Protein Data Bank (PDB, http://www.rscb.org), a molecular model of CYP2B6 was built with the help of refined procedures in order to identify putative active site residues. This model was derived by sequence alignment with the crystallized CYP2B4 which shares the highest sequence homology with CYP2B6 (Scott et al., 2003). Moreover, the crystal structures of CYP2B4 with different ligands more or less bulky revealed its remarkable plasticity (Scott et al., 2003; Scott et al., 2004; Zhao et al., 2006) and demonstrated how the active site of the enzyme can be reshaped to accommodate ligands of different sizes and shapes while maintaining the overall CYP folding. The crystal structure of CYP2B4 (PDB code 1SUO) complexed with the specific inhibitor 4-(4-chlorophenyl) imidazole (CPI) was chosen as a unique template for the rebuilding process. This template is a reasonable choice, since CPA and CPI are substrates of comparable size and chemical structure. After docking CPA into the CYP2B6 homology model, four amino acid residues were identified to be in close contact with the substrate (I114, V367, V477 and G478) and were selected for mutagenesis. For each position, a large variety of amino acids were tested (hydrophobic, polar, charged, neutral side chains).

Second, similar to the human orthologous CYP2B6, several CYP2B isoforms catalyze 4-OH-CPA hydroxylation: CYP2B1 in rat, CYP2B4 and CYP2B5 in rabbit and CYP2B11 in dog (Chen et al., 2004). The activity of rat CYP2B1 was 10 to 35-fold higher than that of rabbit CYP2B4 and CYP2B5, whereas canine CYP2B11, exhibiting a particularly low Km (80-160 µM), was 7- to 8 fold more active than CYP2B1. The primary structure alignment of these different isoforms (Table 1)

Molecular Pharmacology Fast Forward. Published on January 22, 2008 as DOI: 10.1124/mol.107.042861
This article has not been copyedited and formatted. The final version may differ from this version.

suggested few additional positions for site-directed mutagenesis experiments in CYP2B6. We focused on mutations of amino acids that are exclusively present in the CYP2B11 substrate recognition sequences (SRS).

Following both strategies, we designed various single and double mutants obtained by site-directed mutagenesis. These mutants were cloned into the yeast expression vector pYeDP60 (V60) and expressed in *Saccharomyces cerevisiae* (Pompon et al., 1996). Site-directed mutant catalytic activities were evaluated using CPA as substrate. Molecular dynamic (MD) simulations of several model complexes (CPA/wild-type or mutated CYP2B6) were achieved to support interpretation of the observed modifications in catalytic efficiency at the molecular level, through the computed dynamic behavior of the substrate within the active site. At last, the potential possibility to enable a CPA-resistant head and neck cancer cell line (A-253) sensitive towards CPA by the GDEPT strategy was examined. Using the most efficient mutant to metabolize CPA, this strategy was found to be quite effective.

Molecular Pharmacology Fast Forward. Published on January 22, 2008 as DOI: 10.1124/mol.107.042861
This article has not been copyedited and formatted. The final version may differ from this version.

Materials and Methods.

Homology modeling: Structural models of CYP2B6 were first built by homology modeling on the basis of the crystal structure of CYP2B4 using Modeller 7 (Sali and Blundell, 1993) after PDB release of the structure of CYP2B4 co-crystallized with 4-(4-chlorophenyl)imidazole (CPI) in a closed configuration (pdb: 1SUO) (Scott et al., 2004). Thanks to high primary sequence identity between CYP2B6 and CYP2B4 (78%), an unambiguous sequence alignment was generated using Clustal W (Thompson et al., 1994) and submitted as input to Modeller 7. In the rebuilding process, the first 27 N-terminal residues of CYP2B6 were deleted as they had no equivalent in the sequence of the crystallized CYP2B4. In the Modeller topology input file, the parameters for *MD_level* and *Repeat_Optimization* were set, respectively, to "refine_3" and "3". 100 models were generated and the best 20 were kept according to the objective function computed by Modeller, which is a score determined by a combination of parameters used by the program during the calculation and is used to select the best model. Among the 20 models kept, a second scoring was applied using 3 key programs of protein structure quality assessment: ProQ (Wallner and Elofsson, 2003), Anolea (Melo et al., 1997) and Prosa (Sippl, 1993). The final model selected was the best according to a good compromise between the scores calculated by the three programs. For treatment of the heme moiety, which was considered as an additional residue in Modeller, the atomic coordinates of the heme from the CYP2B4 template were directly re-assigned to the CYP2B6 model. For final structure refinement, the selected consensus model was then equilibrated and relaxed using the GROMACS v3.1.4 molecular dynamics simulation package. The attachment of the heme residue to the proximal cysteine in the model was completed by GROMACS script *pdb2gmx*. The Root Mean Square Deviation (RMSD) values

Molecular Pharmacology Fast Forward. Published on January 22, 2008 as DOI: 10.1124/mol.107.042861
This article has not been copyedited and formatted. The final version may differ from this version.

between the different models optimized by MD and the template structure were calculated using the McLachlan algorithm (McLachlan, 1982) as implemented in the protein least squares fitting program ProFit (Martin, A.C.R., http://www.bioinf.org.uk/software/profit/). For detection of cavities and computation of active site volume in the models, the Voidoo program from Uppsala Software Factory (Kleywegt et al., 2006) was applied. Calculation type was set to "C" (for cavity), and type of cavity volume to be calculated was set to "O", i.e. the volume "probe-occupied" or occupied by the rolling probe, that we call hereafter the solvent molecular accessible surface (SMAS). Prior to the computation, water and ligand molecules were removed. Probe solvent radius chosen was 1.4Å and primary grid spacing was set to 0.33Å. Studies of various pathways from the active site to the outside were carried out using the Caver tool (Petrek et al., 2006) (http://loschmidt.chemi.muni.cz/caver/). The grid size value was set to 0.8Å and the starting point for channel searching was specified by XYZ-coordinates of a point located at about 1Å above the heme iron atom. The maximum number of tunnels to be found was set to 5. Channel characterization during the MD trajectory was used for defining putative pathways followed by the substrate and for examining potential effects of mutations in ligand processing by CYP2B6. Representation of CAVER-derived channels was performed using the molecular graphics and modeling package PyMOL (DeLano, W.L. The PyMOL Molecular Graphics System 2002 http://www.pymol.org).

Initial positioning of CPA in the active site of CYP2B6 models: The two enantiomers of the CPA molecule were initially docked into the CYP2B6 model active site using the atomic coordinates derived from the CPI molecule position in the crystallized

Molecular Pharmacology Fast Forward. Published on January 22, 2008 as DOI: 10.1124/mol.107.042861
This article has not been copyedited and formatted. The final version may differ from this version.

CYP2B4 active site. The atoms located in front of the heme iron in CPI (1SUO) and CPA respectively, were superimposed. The CPA substrate was then manually repositioned in CYP2B6 active site to optimize the steric conflicts with side chains present within five Å of the substrate. Residual steric bumps were fixed by a local Powell minimization of 1000 steps carried out in the SYBYL software (Tripos) environment using *Tripos Force Field and Gasteiger-Huckel* charge calculation with a non-bonded energy cutoff of eight Å and a gradient termination of 0.005 kcal/(mol*A). In this step, local minimization under SYBYL was operated with an aggregate defined by the whole protein, including the heme, deprived of a spherical area of 10 Å surrounding the substrate. Global minimization of 1000 steps without constraints was finally performed to generate the final structure of the CYP2B6 model/CPA complex used in subsequent steps.

Mutational work in silico: Mutations were performed *in silico* using the Biopolymer module of the SYBYL 7.1 software (Tripos Inc. St Louis, USA). For each mutation, the side chain conformation was fixed, using selection of the best rotamer for adjustment of side chain positions and local minimization to remove close contacts and locally relax the system. Parameters used for minimization were the same as above. No aggregate was used at this stage and no global minimization was performed since all models were submitted to MD simulation for subsequent docking calculations.

Molecular Dynamics simulations: The structural models of CYP2B6 and the mutants were equilibrated by extensive MD simulations of 2 ns in explicit solvent in the absence and in presence of CPA docked in the active site. All MD simulations were

Molecular Pharmacology Fast Forward. Published on January 22, 2008 as DOI: 10.1124/mol.107.042861
This article has not been copyedited and formatted. The final version may differ from this version.

carried out using the GROMACS v3.1.4 molecular dynamics simulation package (Schulte-Ladbeck et al., 2001). For the generation of topology files under GROMACS, the structure template coordinates file was split into two structure files, one for the protein and one for the ligand, in order to keep the two molecules in the same frame of reference. Protein and CPA coordinates structure files were then separately converted into *gro* file (coordinates) and *top* file (topology file) as input files for GROMACS. The CPA file was converted by the PRODRG server, a utility that provides topology parameters of organic compounds while respecting the coordinates in the initial frame of reference (http://davapc1.bioch.dundee.ac.uk/programs/prodrg/). The protein file was converted by the *pdb2gmx* script using the parameter set ffgmx (GMX force field of Gromos87) which also provides topology parameters for the heme and various cofactors. The topology of the heme residue (HEM) was the default generated by *pdb2gmx*, with a total net charge of -2 for the protoporphyrin IX moiety associated to iron (II). Attachment of the heme to the proximal cysteine residue through cys-thiolate bond was also performed by the *pdb2gmx* script, and all MD simulations were carried out with the heme macrocycle in the penta-coordinated state (5-c), corresponding to the high-spin state of the enzyme before ligand binding. The choice of GMX as a force field was driven by the fact that it is the only force field compatible with GROMACS's ligand topologies obtained from the PRODRG server. In the prodrg script, chirality, full charges and energy minimization flags were respectively set to "*yes-yes-no*". CPA *gro* and *top* files were then merged to the protein files according to the procedure described in Kerrigan's Tutorial for the Drug-Enzyme complex (http:www2.umdnj.edu/~kerrigie). The presence of water molecules in the active site was taken into account by solvation of the complex CYP2B6/CPA in explicit solvent,

Molecular Pharmacology Fast Forward. Published on January 22, 2008 as DOI: 10.1124/mol.107.042861
This article has not been copyedited and formatted. The final version may differ from this version.

using a truncated octahedral periodic box (*editconf* and *genbox* script dimensions of the box based upon setting the box edge 10 Å from the protein, i.e. 92 x 85x 75 $Å^3$). The whole system was then charge-neutralized by adding three counter ions and energy-minimized without restraints for 5000 steps using the steepest minimization to remove residual steric clashes. After minimization, position-restrained MD simulation of 20 ps was performed (protein atoms positions restrained, CPA, solvent molecules and ions not restrained) for equilibration and free diffusion of water molecules into the protein structure. Conditions for MD simulation were: NPT ensemble, the PME (Particle Mesh Ewald) electrostatics method (Darden et al., 1993) for computing long-range electrostatics with a real space cutoff of nine Å, temperature and pressure coupling using Beredsen's algorithm (Berendsen et al., 1984) with temperature of the system fixed at 300 K with a coupling constant constant τ_T = 0.1 ps, and pressure set at one bar with a coupling constant τ_P = 0.5 ps and compressibility set to 4.5×10^5 bar^{-1} in all simulation box directions. Protein, heme, CPA, solvent and ions were coupled separately. The time-step for integration was 2 fs and coordinates and velocities were saved every 0.5 ps. For constrained MD simulations, the all-bond option was set, applying the Linear Constraint algorithm (Hess et al., 1997) to restrain all bond lengths in the system. After this equilibration, unconstrained extensive MD simulations of 2 ns using wild-type or mutants CYP2B6 complexed with CPA were carried out with the same parameters.

Construction of CYP2B6 mutants. Site-directed mutagenesis was based on the QuikChange® kit (Stratagene, Amsterdam, The Netherlands). A single PCR reaction using mutagenic primers and wt V-60CYP2B6 (Gervot et al., 1999) as template was performed followed by *Dpn I* digestion and transformation into competent DH5α

Molecular Pharmacology Fast Forward. Published on January 22, 2008 as DOI: 10.1124/mol.107.042861
This article has not been copyedited and formatted. The final version may differ from this version.

bacteria. The mutagenic PCR program was as follows 10 min at 92°C, followed by 17 cycles at 92°C for 45 sec, 59°C for 45 sec and 68°C for 26 min and a final extension of 10 min at 68°C. All PCR reactions were performed using *Pfu turbo* polymerase (Stratagene). All mutants generated were sequenced by direct sequencing using an automatic Perkin Elmer sequencer in order to be sure that the desired mutant was obtained.

Expression in yeasts. The yeast expression plasmid pYeDP60 and the W(R) *Saccharomyces Cerevisiae* strain, constructed by substitution of the natural W303-1B yeast reductase promoter by the galactose inducible GAL10-CYC1 hybrid promoter, (Truan et al., 1993) were gifts from D. Pompon (Gif-sur-Yvette, France).

Mutated and wild type CYP2B6 were expressed in the W(R) yeast strain, in which yeast NADPH cytochrome P450 reductase was over-expressed. The pYeDP60 plasmid was introduced into intact yeast cells based on a refined LiAc-mediated protocol (Truan et al., 1993). Yeast culture conditions have been previously described (Bellamine et al., 1994).

Cell line. Human A-253 epidermoid carcinoma cells from the submaxillary gland (ATCC-HTB 41), purchased from LGC Promochem (Molsheim, France), were grown as a monolayer in Dulbecco's modified Eagle minimum essential medium (MEM) supplemented with 10 % fetal bovine serum (FBS), non essential amino acids for MEM, penicillin at 200 U/ml and streptomycin at 50µg/ml.

Preparation of the yeast microsomal fraction. Yeast microsomes were prepared based on the mechanical disruption method using glass beads as described

Molecular Pharmacology Fast Forward. Published on January 22, 2008 as DOI: 10.1124/mol.107.042861
This article has not been copyedited and formatted. The final version may differ from this version.

elsewhere (Bellamine et al., 1994). The yeast microsomal protein concentration was determined by the Pierce bicinchoninic acid (BCA) procedure according to the manufacturer's instructions using bovine serum albumin as a standard. Microsomal CYP content was spectrally determined by the method of Schoene et al. (Schoene et al., 1972).

Recombinant adenovirus. CYP2B6, human cytochrome P450 reductase (RED) and the double mutant CYP2B6 114V/477W provided by our laboratory were sent to the University Hospital of Nantes supported by the Association Française contre les myopathies (AFM) and cloned into serotype five adenovirus (http://www.vectors.nantes.inserm.fr/). A replication defective E1 and E3 region-deleted adenovirus encoding CYP2B6, human RED and the 2B6 double mutant were constructed and purified, and the titer was determined spectrophotometrically.

CPA 4-hydroxylase activity. The fluorometric determination of microsomal CPA 4-hydroxylase was adapted from a technique previously described (Roy et al., 1999) for a 96-well microplate with several modifications. Incubations were carried out for one hour at 28°C in a total volume of 200 µl and included 100 mM sodium phosphate buffer, pH 7.4, 1 mM EDTA, 10 pmol of CYP2B6 and 10mM CPA. Reactions were initiated by adding the NADPH-generating system, and stopped by the addition of 200µl of 10% trichloroacetic acid. After centrifugation at 13 000 g and 4°C for 15 min. to pellet the proteins, 300µl of the supernatant was transferred to a clean test tube containing 160 µl of the fluorescence mixture (6 mg of 3-aminophenol and 6 mg of hydroxylamine hydrochloride freshly dissolved in 1ml of 1N HCl). Samples were heated at 90°C for 20 min. to form 7-hydroxyquinoline by condensation of the 4-

Molecular Pharmacology Fast Forward. Published on January 22, 2008 as DOI: 10.1124/mol.107.042861
This article has not been copyedited and formatted. The final version may differ from this version.

hydroxy-CPA with 3-aminophenol. After cooling to room temperature, fluorescence reading were performed on a Bio-tek FL600 microplate fluorescence reader (excitation at 350 nm and emission at 515 nm). Under these assay conditions, product formation was linear with time and the enzyme concentration and amount of 4-hydroxy-CPA under these assay conditions was determined based on a standard curve of 4-hydroxy-CPA (0-20µM) incubated with bovine serum albumin and treated in parallel under the same assay conditions.

The kinetic constants of cyclophosphamide hydroxylase were determined by a non-linear regression with fifteen substrate concentrations (0.05 to 25 mM). Data were analyzed using GraphPad Prism Software (GraphPad Software,inc.) to calculate kinetic parameters (Km, Vmax), with Vmax values expressed as moles of product formed per minute, normalized to the moles of CYP included in each reaction (turnover number expressed as min^{-1}). Data shown were based on duplicate determinations for each data point.

Adenoviral infections and in-vitro cytotoxicity assays. A-253 cells were seeded in six-well plates at 400 000 cells/well. After 24 hours, they were infected for four hours with adenovirus at a multiplicity of infection (MOI) of 300, i.e. number of infectious particles/cell, in cell culture medium containing 2 % FBS. In the case of double infection (Ad-2B6 + Ad-Red) cells were infected with a total of 300 MOI (150 + 150), whereas Ad-LacZ at 150 MOI was used in combination with Ad-2B6 or Ad-Red (150 MOI) to get an even MOI concentration in each well. Cells infected with an adenoviral vector expressing LacZ at 300 MOI were used as a control. No toxicity of the control vector Ad-LacZ was observed at this dose in cells that were not treated with CPA. After 4 hours, the adenovirus-containing medium was removed and replaced with the

Molecular Pharmacology Fast Forward. Published on January 22, 2008 as DOI: 10.1124/mol.107.042861
This article has not been copyedited and formatted. The final version may differ from this version.

usual medium. Overexpression of the transgenes was checked 3 days after infection by western blot using a polyclonal anti-CYP2B6 antibody (Gervot et al., 1999) and a polyclonal anti-rat RED antibody (Daïchi pure chemicals Co. Ltd, Japan) which cross reacts strongly with human RED (data not shown).

For the *in vitro*-cytotoxicity assays, cells were trypsinized 20 hours after infection and plated in a 96-well plate at a concentration of 10 000 cells/well. After 24 hours, they were treated with cyclophosphamide at 0-3 mM concentrations for six days. The cytotoxicity of CPA was measured with a MTS-colorimetric assay, using the "Celltiter 96® Aqueous One Solution Cell Proliferation Assay" (Promega) according to the manufacturer's instructions. Cell viability was calculated as the ratio of the absorbance measured in infected cells to that measured in cells infected with the control (Ad-Lac Z) which were treated with identical CPA concentrations and then calculated as the percentage of the ratio obtained in untreated cells. Assays were repeated four times in triplicate.

NADPH cytochrome P450 reductase (RED) activity assay. RED activity was measured in the cellular microsomal fraction. The NADPH-dependent reduction of cytochrome *c* by RED was assayed as previously described (Yasukochi et al., 1980).

Molecular Pharmacology Fast Forward. Published on January 22, 2008 as DOI: 10.1124/mol.107.042861
This article has not been copyedited and formatted. The final version may differ from this version.

Results

CYP2B6 modeling: The three-dimensional structure of CYP2B6 was generated by homology modeling based on the CYP2B4 structure as a unique template with 78% of sequence identity (Table 1). With such homology, the resulting model of CYP2B6 produced by Modeller 7 according to the Modeller objective function can be considered as a high quality model as assessed by the structure-quality checking programs used (ProQ, Anolea, Prosa). Moreover, the template used was an energetically optimized structure of CYP2B4 for improvement of side chain contacts and rotamer states in the initial pdb structure (1SUO). This relaxed structure of the template was obtained after equilibration in a water box of 1SUO and relaxation by 2ns of MD simulation as described in the materials and methods. As shown by the RMSD values of the backbone atom positions (Fig. 1), the minimized CYP2B6 model (red trace) proved to be very stable during dynamics production at 300K after the first 250 ps of equilibration. For comparison, the MD trajectory is shown for the minimized crystal structure of CYP2B4 (1SUO, black trace), which was performed to generate the optimized template for CYP2B6 rebuilding. RMSD values of the backbone atom positions were calculated between trajectory structures and the starting structure (minimized 1SUO CYP2B4 and minimized CYP2B6 model, respectively). For both structures, the same tendency in the time evolution of RMSD values was observed: a plateau at around 1.8 Å was rapidly reached (within 250 ps for CYP2B6 and 500 ps for CYP2B4), and the structures were then stabilized in their respective conformation all the way to 2 ns. CYP2B6 reaches its equilibrium conformation in a shorter period of time as compared to CYP2B4, because it was generated starting from a 2 ns-optimized MD template and not directly from a crystal structure. For CYP2B4, the observed stabilization at around 1.8 Å RMSD from the starting point (crystal

Molecular Pharmacology Fast Forward. Published on January 22, 2008 as DOI: 10.1124/mol.107.042861
This article has not been copyedited and formatted. The final version may differ from this version.

structure) can be considered as standard in this kind of simulation in explicit solvent at 300K. For CYP2B6, considering the fact that the starting point was a MD-relaxed model, the RMSD profile indicates that the CYP2B6 model reached an equilibrium conformation that is not a strict copy of the template backbone from which it was designed. Indeed, the RMSD value of the backbone atom positions between the two final structures was found at 1.77Å by ProFit (calculated on 464 aligned residues between CYP2B4 and CYP2B6) revealing distinct configurations. These results are in favor of i) good stability and conservation of the global fold within the CYP2B subfamily (no detectable drift after 2 ns of MD simulation, no significant fold divergence whereas CYP2B4 and CYP2B6 differ by more than 100 residues) and ii) accuracy and stability of the CYP2B6 structural model.

Features of the binding site. To characterize the geometry of the binding site, the Voidoo program was applied to calculate the solvent molecular accessible surface (SMAS) in both structures after minimization as well as after MD simulation of 2 ns. In each case, CYP2B6 displayed a larger active site as compared to CYP2B4 accounting in part for the RMSD found between the backbones. According to Voidoo, the crystal structure (not minimized) of CYP2B4 displayed a volume defined by SMAS of 271 $Å^3$, which corresponds to a quite narrow active site in CYP superfamily. When the structure was relaxed by MD in explicit solvent, the volume was found almost unchanged at 252 $Å^3$. Conversely, CYP2B6 model displayed a SMAS volume of 363 $Å^3$, a volume consistent with the binding of ligands bulkier than CPI, such as CPA. The three main sub-pockets described in a previously published model (Bathelt et al., 2002) are also present in our optimized model and are formed by the same residues (Phe206, Ala298, Thr302, Leu363 for pocket A or heme pocket; Ile114,

Molecular Pharmacology Fast Forward. Published on January 22, 2008 as DOI: 10.1124/mol.107.042861
This article has not been copyedited and formatted. The final version may differ from this version.

Phe115, Ser294 and Phe 297 for pocket B, Ile209, Val367 and Val477 for pocket C) with the exception of residue Leu216 (in C pocket) which we found was not oriented towards the active site.

Initial positioning CPA in the active site of CYP2B6 model: The position of the CPI substrate in the CYP2B4 crystal structure 1SUO was used as an initial guess regarding the position of CPA in the active site of CYP2B6 rebuilt models. However, due to the difference in shape and volume between the two compounds and between the two active sites, it was necessary to adjust the position of the CPA for further MD calculations. In particular, the existence of a chiral center in the CPA molecule was taken into account. As no experimental data on the effect of CPA stereochemistry on biological activity were available, the two enantiomers were treated separately in the simulations. The position of the CPI ring close to the heme iron was used as a template to produce the initial positioning of CPA in the CYP2B6 active site. The metabolic (or inhibitory) atom sites of each molecule were superimposed (Fig. 2) and the CYP2B6 structure docked with CPA was relaxed by MD simulation (2ns). Given that CPA displays a chiral center, initial positioning of both enantiomers were performed. The position of the ring of the two enantiomers relative to the heme was unchanged, and the chirality resulted mainly in the inversion of CPA C4 and C6 positions in front of the heme (by symmetry around the P2-C5 axis of the ring). After relaxation, in both cases, C4 and C5 atoms of CPA displayed the shortest distances to the heme iron. All MD trajectories were duplicated with R- and S-enantiomers. The three C atoms of the ring (C4, C5 and C6) exhibited variable distances with respect to heme iron during the 2 ns dynamics simulation, but the average tendency supports dominant metabolism leading to C4 hydroxylation for both enantiomers." The last

Molecular Pharmacology Fast Forward. Published on January 22, 2008 as DOI: 10.1124/mol.107.042861
This article has not been copyedited and formatted. The final version may differ from this version.

structure (2 ns) of each simulation has been minimized under Gromacs force field (500 steps, converged). In the wild type, the following distances have been found: i) S-enantiomer C4-Fe=4.35Å, C5-Fe=4.1Å, C6-Fe=4.5Å, ii) R-enantiomer C4-Fe=6.0Å, C5-Fe=5.6Å, C6-Fe=6.6Å. This would slightly favors the metabolism of S as compared to R, but the differences, to our opinion, are not significant enough to allow such an interpretation.

In the CYP2B6/CPA computed model, CPA is surrounded by 16 residues located within five Å of one another: Val104, Ile110, Ile114, Phe115, Phe206, Phe208, Ile209, Phe297, Ala298, Glu301, Thr302, Ser320, Leu363, Val367, Val477 and Gly478. These residues are at the edge of the active site and most of them have been shown to be important for substrate metabolism (Zhao and Halpert, 2006). Figure 3 shows some of these residues potentially involved in the recognition or positioning of CPA in the active site, as seen after 2ns MD simulation of the complex.

Active site access: The access channels to the active site in the CYP2B6 model were explored using CAVER, a tool providing pathways leading from buried cavities to the outside solvent. CAVER was applied to various structures collected along the MD trajectory of 2 ns. As a result, three main entrance/exit pathways were detected in CYP2B6 (Fig. 4). A first group of channels (orange/red on figure 4) was found close to the B' helix, on both sides of the B-C loop, a region known to be very flexible, adopting different conformations that follow the nature of the bound substrate (Honma et al., 2005). Depending on the frame of the simulation, several pathways of variable importance emerged in this region. The variability of the channel position around the B' helix was clearly dependent upon the conformation of the B-C loop during the MD trajectory. A second pathway (blue, figure 4) was found between the

Molecular Pharmacology Fast Forward. Published on January 22, 2008 as DOI: 10.1124/mol.107.042861
This article has not been copyedited and formatted. The final version may differ from this version.

E, F and I helices and the ß-turn of $ß_4$ sheet. Similar to the first pathway, its relative importance was dependent on the frame of the MD going from a widely open state to an almost closed state. The third pathway (purple, figure 4) was found positioned between A, I and K helices, along helix I.

All these pathways have been described in the survey by Cojocaru et al. (Cojocaru et al., 2007), and our first, second and third pathways correspond to channel (subclasses a, b, c, ac, e), channel S (or solvent channel) and channel five, respectively. In CYP2B6, the main access is thus represented by three channels lined by the B-C loop/B'-Helix that alternate dynamically. This adaptability is not surprising in a region of the protein structure known to be highly variable in sequence and structure between different CYPs and is important for substrate recognition and specificity. Regarding the S channel, the egress between E, F, I helices and the $ß_4$ turn is frequently found in the CYP superfamily (Cojocaru et al., 2007). Conversely, channel five is a particular access of unknown role and found in only few structures of CYP including CYP2B4. The three same channels were found in the relaxed CYP2B4 structure indicating similar pathways for substrates in both enzymes, despite differences in their active sites.

CYP2B6 mutagenesis. A total of twenty-six CYP2B6 site-directed mutants were constructed, as tabulated in Table 2. In all cases, the entire CYP2B6 coding sequence was checked to ensure that the expected base changes had been performed and that no undesired mutations were introduced during the process of site-directed mutagenesis. The twenty-six mutants are shared between i) active site mutations at four positions as suggested by the modeling (114, 367, 477, 478, nineteen single mutants and one double mutant) and ii) canine-derived mutations at

Molecular Pharmacology Fast Forward. Published on January 22, 2008 as DOI: 10.1124/mol.107.042861
This article has not been copyedited and formatted. The final version may differ from this version.

six positions as suggested by CYP2B SRS alignment of Table 1 (107, 199, 207, 236, 365, 475, all single mutants. The six "canine" mutants were constructed to replacie related amino acids in human CYPB6 with amino acids exclusively present in canine CYP2B11 (F107V, L199M, S207A, K236N, M365I and C475I).

Heterologous expression of CYP2B6 constructs. All CYP2B6 site-directed mutants were successfully expressed in yeast microsomes. The levels of CYP expression spectrally determined show large variations from one construct to the other (ranging from 17 to 340 pmol/mg of microsomal protein) (Table 2). Interestingly, spectral CYP expression was comparable in yeasts expressing wt CYP2B6 or the double mutant I114V/V477W. However, catalytic enzyme assays have been performed using the same amount of active CYP content for each construct and, therefore, were not affected by the various levels of expression.

Enzyme Kinetic analysis. All mutants were investigated for CPA 4-hydroxylase activity in order to determine their kinetic parameters; Vmax, Km and Vmax/Km ratio of CPA-4'hydroxylation by CYP2B6. The site-directed mutants are presented in Table 2 and a typical graphical analysis is displayed figure 5.

The first part of Table 2 displays the results obtained by mutations in the active site. I114V substitution increased the CPA-4OH efficiency (Vmax/Km) mainly by decreasing the Km (-50%) of this activity. Amino acid V367 was mutated into L, F, S, T and H. An increase in Vmax was only observed with the V367L mutant, however, due to the Km increase, the catalytic efficiency of this mutant remained slightly lower than that of the wild-type CYP2B6. All other mutants at position 367 resulted in much lower CPA-4 hydroxylase activity (43 to 2% of wild-type CYP2B6). The substitution of

Molecular Pharmacology Fast Forward. Published on January 22, 2008 as DOI: 10.1124/mol.107.042861
This article has not been copyedited and formatted. The final version may differ from this version.

V477 with S, T, Y, N, D and E also proved to be also detrimental for CPA-4OH hydroxylase activity. This activity was undetectable in V477N and V477S mutants. In contrast, replacement of V with hydrophobic and aromatic amino acids resulted in a significant increase in CPA-4OH catalytic efficiency which was directly correlated with the size of the side chain (I (x1.89) <F (1.91) <W (x2.78). Replacement of G478 with A, V, S and E significantly reduced CPA-4OH hydroxylase activity from 36 to 5% of wild-type CYP2B6.

In the “canine” series (Table 2), only the L199M mutant showed a two-fold increase in catalytic efficiency to metabolize CPA in 4-OH-CPA. However, the affinity of the six “canine” mutants remained comparable or lower than that of the wild type CYP2B6.

From the results obtained with the different mutants, the construction of a new mutant, comprising the two mutations that proved to be most effective for metabolism of CPA (I114V and V477W) was undertaken. As shown in the last line of Table 2, this double mutant I114V/V477W showed a four-fold increase in CPA-4OH catalytic efficiency, mainly due to an increase in enzyme affinity.

Comparison of the active site between wt CYP2B6 and CYP2B6 V477W/I114V: Structural models were built to provide an interpretation of the variations observed in biological activities. One can notice that the replacement of residue V477 which is positioned on the top edge of the active site in wild type CYP2B6 with a tryptophanyl residue in the double mutant (Fig. 6) yielded a local lateral contraction of the cavity. Indeed, due to side chain increased volume at position 477, the mutation led to a steric hindrance that provoked displacement of the ligand in the active pocket by stacking it against helix I. In addition, mutation of I114 to a valine, located on the

Molecular Pharmacology Fast Forward. Published on January 22, 2008 as DOI: 10.1124/mol.107.042861
This article has not been copyedited and formatted. The final version may differ from this version.

lateral side near the bottom of the active site (BC loop), caused a widening in the vicinity of the heme. This double mutation forced a tilt of the CPA from its initial position. This observed tilt of the CPA provided a better positioning of the CPA over the three above-mentioned pockets. The volume of the mutated active site, as calculated by Voidoo, increased to 636 $Å^3$, a value that also reflects an extension towards the channels at the top. The same steric guidance effect was observed for both enantiomers.

Dynamic behaviour of the CPA in the active site of wt CYP2B6 versus V477W/I114V CYP2B6 (Fig. 7): The dynamic behavior of the substrate within the active site can be followed by analysis of the time evolution of all RMSD atoms during the MD simulation. Figure 7 shows RMSD fluctuations of CPA (S-enantiomer) during 2 ns of MD, as computed by GROMACS. At the plateau (reached at 100 ps for the mutant and 600 ps for the wild type), RMSD amplitudes reflect the deviation from the average position of the substrate. The R-enantiomer showed the same overall differential tendency (data not shown), although it was found more fluctuating in the active site than the S-enantiomer, both in the wild type and in the double mutant simulations. Figure 7 shows that the RMSD fluctuations of CPA (S-enantiomer) are significantly restricted in the mutant model as compared to the wild type. Therefore, CPA showed restrained mobility in the mutant. It has to be mentioned that the levels of RMSD were dependent upon the initial positioning and therefore are not relevant as absolute values.

In vitro cytotoxicity assays: Preliminary experiments showed that A-253 cells, originated from head and neck epidermoid carcinoma, remained insensitive to CPA treatment up to 3 mM (data not shown). CYP2B6 was not expressed in this cell line

Molecular Pharmacology Fast Forward. Published on January 22, 2008 as DOI: 10.1124/mol.107.042861
This article has not been copyedited and formatted. The final version may differ from this version.

and RED activity remained relatively weak (12.1 ± 1,5 nmol/min/mg). Results of the *in vitro* cytotoxicity assays are summarized in Figure 8. No cytotoxicity was observed after treatment of Ad-LacZ infected cells with up to 3 mM CPA. Infection of cells with Ad-RED alone or with Ad-2B6 alone did not result in any cytotoxic effects in the A-253 cell line at any CPA concentration used. At 3 mM CPA, infection with the adenovirus expressing the double mutant V477W/I114V alone or in association with Ad-RED led to a cytotoxic effect of CPA. This cytotoxic effect increased with the CPA concentration, reaching 70% at 3 mM.

Molecular Pharmacology Fast Forward. Published on January 22, 2008 as DOI: 10.1124/mol.107.042861
This article has not been copyedited and formatted. The final version may differ from this version.

Discussion

Local metabolism of a prodrug within tumor cells provides a potential mechanism for delivering high local concentrations of the active metabolites while minimizing systemic drug concentrations and, thus, toxicity. The concept of overexpressing individual forms of prodrug-metabolizing CYP enzymes in tumor cells is now becoming well recognized (McFadyen et al., 2004), in particular the CYP2B6/CPA strategy (Jounaidi, 2002; Tychopoulos et al., 2005; Waxman et al., 1999). However, one of the major drawbacks of this strategy, is the relatively low affinity of CYP2B6 for CPA. The present work was then undertaken to improve the catalytic activity of CYP2B6 for activation of CPA by site-directed mutagenesis using a rebuilt structural model of CYP2B6.

MD simulations demonstrated that the stability of CYP2B4 and the constructed model of CYP2B6 were comparable, as evidenced by time evolution of RMSD (Fig. 1), which strengthens the choice of CYP2B4 as a unique template for homology modeling. CYP2B4 was co-crystallized with CPI (Scott et al., 2004) which can be considered as structurally close to CPA (Fig. 2). In all MD simulations that were carried out, the final position of CPA in the active site was always the same, and not dependent upon its initial manually created position. Although CPA displays a chiral center, no data were available in the literature about the respective biological activities and metabolism of R ans S enantiomers thus preventing comparison with results obtained *in silico*. Nevertheless all simulations were duplicated for R- and S-CPA and showed no marked difference between the two enantiomers in the average position in the active site and in the potential metabolism resulting from the position metabolism. Given that a racemic mixture is always used in clinical therapy, we chose not to emphasize this point of discussion in this work .

Molecular Pharmacology Fast Forward. Published on January 22, 2008 as DOI: 10.1124/mol.107.042861
This article has not been copyedited and formatted. The final version may differ from this version.

Some CYP2B6 active site residues have already been subjected to site-directed mutagenesis (Domanski et al., 1999; Spatzenegger et al., 2003). For example, the V477F CYP2B6 mutant has been reported to have increased catalytic activity for 7-ethoxycoumarin (7-EC) (2.1-fold increase) and 7-ethoxy-4-trifluoromethylcoumarin-O-deethylase (7-EFC) (1.8-fold increase). From our CYP2B6 model, we selected amino acids close to the substrate (I114, V367, V477 and G478) to build a range of mutants. Our initial goal was to stabilize the substrate in the active site pocket by hydrogen bonding and, thus, hydrophobic amino acids V367, V477 and G478 were mutated into polar amino acids that could establish hydrogen bonds with the substrate (V367S, V367T, V367H, V477S, V477T, V477Y, V477N, V477D, V477E, G478S, G478E). The results showed that the introduction of polar amino acids into the active site was often detrimental for catalytic activity; this result highlighted that it was necessary to preserve the global hydrophobic nature of the active site.

In addition, replacement of these residues with hydrophobic amino acids gave contrasting results for CPA-4' hydroxylase activity depending on the amino acid considered. Substitution of V367 with F or G478 with A decreased this activity whereas substitution of V367 with L or G478 with V showed no significant effect on this activity. In contrast, mutants more efficient than wt CYP2B6 were obtained by replacement of V477 with I, F and W leading to a decrease in the Km and an increase in the Vmax of CPA-4' hydroxylase activity (Table 2). The CYP2B6 active site was found to be relatively large (as compared to CYP2B4), allowing for amplified CPA motions inside. For instance the two aliphatic chains (CH_2CH_2Cl) can rotate around a virtual axis defined by the CPA acyclic P-N bond and can also freely tilt up

Molecular Pharmacology Fast Forward. Published on January 22, 2008 as DOI: 10.1124/mol.107.042861
This article has not been copyedited and formatted. The final version may differ from this version.

and down. Replacement of V477 with bulky residues restricted these motions, and this restraint was correlated with the size of the residue (V477I, V477F, V477W, table 2), the most efficient being the V477W mutant. In this latter mutant, the steric control exerted by the mutated side chain could allow for more effective presentation of the hydroxylation site to the iron of the heme by reducing the number of statistically non productive orientations. This is supported by the observed increase in affinity, and higher metabolism efficiency.

Moreover, when comparing CPA hydroxylase activities between V477Y and V477F, our results confirmed that in addition to the size of the residue, which is comparable between tyrosine and phenylalanine, its hydrophobicity was essential to maintain enzymatic activity. Indeed, in the V477Y mutant, it was observed, by MD simulations, both with and without CPA, that the hydroxyl group of the tyrosine can occasionally establish a stable H-bond with the glutamic acid (E301) (Fig. 9). In the V477Y mutant, the E301 side chain is reoriented towards Y477 on the top of the active site, and this locking mechanism could hinder the entrance/egress of the CPA. According to CAVER analysis, the two channels located next to the F helix and along the I helix (blue and purple, figure 4) can be closed by this 477/301 H-bond in the mutant.

The last “active site” mutation investigated (I114) also involved a possible gating of the other group of access channels (red/orange in figure 4). Replacement of I114 with a less bulky hydrophobic residue (valine) yielded enhanced catalytic activity (Table 2). In fact, this effect can be related to the key position of this residue on the B’-C loop by promoting CPA accessibility to the active site through the major pathway (channel 2 class in R. Wade nomenclature, (Cojocaru et al., 2007)).

Molecular Pharmacology Fast Forward. Published on January 22, 2008 as DOI: 10.1124/mol.107.042861
This article has not been copyedited and formatted. The final version may differ from this version.

Given that canine CYP2B11 presented a higher affinity for CPA (Chen et al., 2004), a set of six mutants were built up by introduction in CYP2B6 SRS sequences of residues exclusively present in CYP2B11. Unfortunately, none of them exhibited improved affinity to CPA and the Km of K236N was even 10-fold higher than that of in wt CYP2B6 (Table 2). This latter effect can be related to the position of the K236 side chain in the structure of CYP2B6. Indeed, this residue was found located in the G helix, outside of the active site. This structural region (F-G loop and F and G helices) is, according to hydrophobicity surface potential (data not shown) and other literature arguments, thought to be located at the membrane interface. As the lysyl side chain was found oriented towards the outside, i.e. potentially towards the membrane, the substitution with asparagine may perturb the interaction with lipids. As this interaction is likely to influence movements of the F-G crown and access to substrates from the lipid phase, such a mutation can have consequences in CYP activity modulation by membrane, and affect substrate metabolism.

Nevertheless, among the six “canine” mutants, one mutant, L199M, proved to be more efficient than wt CYP2B6 in CPA metabolism. In this case, the mutation is located in a region of the F helix involved in helix-helix contacts with the E helix. Leucine is replaced with a polar residue that can establish new interactions with vicinal side chains on the E helix, either Q172 or S173, which are close enough to establish H-bonds with 199M, thus leading to rigidifying of the E-F scaffold. Such a motional restriction can once again generate improved channeling for the substrate, and thus improved catalytic efficiency.

The double mutant, which contains the two most efficient mutations, I114V and V477W, showed an additive four-fold increase in 4’-hydroxylation of CPA, mainly due to an increase in enzyme affinity. In figure 6, the active site in the double mutant,

Molecular Pharmacology Fast Forward. Published on January 22, 2008 as DOI: 10.1124/mol.107.042861
This article has not been copyedited and formatted. The final version may differ from this version.

compared to wt CYP2B6 is deviated and narrowed at the top, leading to stacking of CPA against the I helix, and becomes wider at the basis of the active site in the vicinity of the heme moiety; as a result, the double mutation forced a tilt of the CPA from its initial position. A possible consequence of this steric displacement is a restricted motion of the substrate in the active site pocket, thus allowing for longer presentation of its metabolic site to the heme iron. Moreover, as indicated by RMSD amplitudes (Fig. 7), CPA appeared to be less mobile in the mutant structural model. This restrained motion could favor higher metabolism efficiency (see supplemental data).

To complete our work, *ex vivo* cytotoxicity assays were performed on the A-253 cell line currently used as a prototype of squamous cells from human head and neck cancer (Kawakami et al., 2001). Wt CYP2B6 or the double mutant CYP2B6 V114/W477 alone or in combination with RED were expressed into A253 cells using adenoviral vectors. Coexpression of CYP2B6 and RED led to a maximum cytotoxicity of 25% which is much lower than that observed in previous studies using lung cancer cells (Tychopoulos et al., 2005) or gliosarcoma cells (Jounaidi, 2002). However, expression of the CYP2B6 mutant led to a substantial increase in CPA-induced cytotoxicity, which could be observed at lower CPA concentrations in these cells compared to cells transfected with wt CYP2B6. This cytotoxicity was dose-dependent and reached 75% at 3 mM of CPA. Coexpression of RED with the CYP2B6 mutant did not increase CPA cytotoxicity compared to cells infected with the CYP2B6 mutant alone. This can be explained by a higher efficiency of electron transfer from the weakly expressed endogenous RED to the CYP2B6 mutant than to wt CYP2B6. This hypothesis, however, remains to be demonstrated.

In conclusion, this work demonstrated that it was possible to improve the

Molecular Pharmacology Fast Forward. Published on January 22, 2008 as DOI: 10.1124/mol.107.042861
This article has not been copyedited and formatted. The final version may differ from this version.

activity of CYP2B6 towards CPA by site-directed mutagenesis. Moreover, from our constructed model of CYP2B6, MD simulations were found to be consistent with the observed modifications in catalytic efficiency of different mutants, and showed their ability to guide the design of new mutants. Given the encouraging results obtained, this study will be pursued by evaluating our strategy *in vivo* against subcutaneous A-253 tumor xenografts in athymic mice of advanced tumor stage. According to the results obtained in this *in vivo* model, clinical protocols could be undertaken.

Molecular Pharmacology Fast Forward. Published on January 22, 2008 as DOI: 10.1124/mol.107.042861
This article has not been copyedited and formatted. The final version may differ from this version.

References

Ayash LJ, Wright JE, Tretyakov O, Gonin R, Elias A, Wheeler C, Eder JP, Rosowsky A, Antman K and Frei E, 3rd (1992) Cyclophosphamide pharmacokinetics: correlation with cardiac toxicity and tumor response. *J Clin Oncol* **10**(6):995-1000.

Bathelt C, Schmid RD and Pleiss J (2002) Regioselectivity of CYP2B6: homology modeling, molecular dynamics simulation, docking. *J Mol Model* **8**(11):327-335.

Bellamine A, Gautier JC, Urban P and Pompon D (1994) Chimeras of the human cytochrome P450 1A family produced in yeast. Accumulation in microsomal membranes, enzyme kinetics and stability. *Eur J Biochem* **225**(3):1005-1013.

Berendsen HJC, Postma JPM, Van Gunsteren WF, DiNola A and Haak JR (1984) Molecular dynamics with coupling to an external bath. *Journal of Chemical Physics* **81**:3684-3690.

Braybrooke JP, Slade A, Deplanque G, Harrop R, Madhusudan S, Forster MD, Gibson R, Makris A, Talbot DC, Steiner J, White L, Kan O, Naylor S, Carroll MW, Kingsman SM and Harris AL (2005) Phase I study of MetXia-P450 gene therapy and oral cyclophosphamide for patients with advanced breast cancer or melanoma. *Clin Cancer Res* **11**(4):1512-1520.

Chen CS, Lin JT, Goss KA, He YA, Halpert JR and Waxman DJ (2004) Activation of the anticancer prodrugs cyclophosphamide and ifosfamide: identification of cytochrome P450 2B enzymes and site-specific mutants with improved enzyme kinetics. *Mol Pharmacol* **65**(5):1278-1285.

Cojocaru V, Winn PJ and Wade RC (2007) The ins and outs of cytochrome P450s. *Biochim Biophys Acta* **1770**(3):390-401.

Darden DA, York DM and Pedersen LG (1993) *J Chem Phys* **98**:10089-10092.

Domanski TL and Halpert JR (2001) Analysis of mammalian cytochrome P450 structure and function by site-directed mutagenesis. *Curr Drug Metab* **2**(2):117-137.

Domanski TL, Schultz KM, Roussel F, Stevens JC and Halpert JR (1999) Structure-function analysis of human cytochrome P-450 2B6 using a novel substrate, site-directed mutagenesis, and molecular modeling. *J Pharmacol Exp Ther* **290**(3):1141-1147.

Gervot L, Rochat B, Gautier JC, Bohnenstengel F, Kroemer H, de Berardinis V, Martin H, Beaune P and de Waziers I (1999) Human CYP2B6: expression, inducibility and catalytic activities. *Pharmacogenetics* **9**(3):295-306.

Goren MP, Wright RK, Pratt CB and Pell FE (1986) Dechloroethylation of ifosfamide and neurotoxicity. *Lancet* **2**(8517):1219-1220.

Hess B, Bekker H, Berendsen HJC and Fraaije JGEM (1997) LINCS: A linear constraint solver for molecular simulations. *Journal of Computational Chemistry* **18**:1463-1472.

Honma W, Li W, Liu H, Scott EE and Halpert JR (2005) Functional role of residues in the helix B' region of cytochrome P450 2B1. *Arch Biochem Biophys* **435**(1):157-165.

Jounaidi Y (2002) Cytochrome P450-based gene therapy for cancer treatment: from concept to the clinic. *Curr Drug Metab* **3**(6):609-622.

Kawakami K, Kawakami M, Joshi BH and Puri RK (2001) Interleukin-13 receptor-targeted cancer therapy in an immunodeficient animal model of human head and neck cancer. *Cancer Res* **61**(16):6194-6200.

Kleywegt GJ, Zou J-Y, Kjeldgaard M and Jones TA (2006) *International Tables for Crystallography*.

McFadyen MC, Melvin WT and Murray GI (2004) Cytochrome P450 enzymes: novel options for cancer therapeutics. *Mol Cancer Ther* **3**(3):363-371.

McLachlan AD (1982) Rapid comparison of protein structures. *Acta Cryst* **A38**:871-873.

Melet A, Assrir N, Jean P, Pilar Lopez-Garcia M, Marques-Soares C, Jaouen M, Dansette PM, Sari MA and Mansuy D (2003) Substrate selectivity of human cytochrome P450 2C9: importance of residues 476, 365, and 114 in recognition of diclofenac and sulfaphenazole and in mechanism-based inactivation by tienilic acid. *Arch Biochem Biophys* **409**(1):80-91.

Melo F, Devos D, Depiereux E and Feytmans E (1997) ANOLEA: a www server to assess protein structures. *Proc Int Conf Intell Syst Mol Biol* **5**:187-190.

Peters WP, Ross M, Vredenburgh JJ, Meisenberg B, Marks LB, Winer E, Kurtzberg J, Bast RC, Jr., Jones R, Shpall E and et al. (1993) High-dose chemotherapy and autologous bone marrow support as consolidation after standard-dose adjuvant therapy for high-risk primary breast cancer. *J Clin Oncol* **11**(6):1132-1143.

Petrek M, Otyepka M, Banas P, Kosinova P, Koca J and Damborsky J (2006) CAVER: a new tool to explore routes from protein clefts, pockets and cavities. *BMC Bioinformatics* **7**:316.

Pompon D, Louerat B, Bronine A and Urban P (1996) Yeast expression of animal and plant P450s in optimized redox environments. *Methods Enzymol* **272**:51-64.

Roy P, Yu LJ, Crespi CL and Waxman DJ (1999) Development of a substrate-activity based approach to identify the major human liver P-450 catalysts of cyclophosphamide and ifosfamide activation based on cDNA-expressed activities and liver microsomal P-450 profiles. *Drug Metab Dispos* **27**(6):655-666.

Sali A and Blundell TL (1993) Comparative protein modelling by satisfaction of spatial restraints. *J Mol Biol* **234**(3):779-815.

Schoene B, Fleischmann RA, Remmer H and von Oldershausen HF (1972) Determination of drug metabolizing enzymes in needle biopsies of human liver. *Eur J Clin Pharmacol* **4**(2):65-73.

Schulte-Ladbeck R, Lindahl R, Levin JO and Karst U (2001) Characterization of chemical interferences in the determination of unsaturated aldehydes using aromatic hydrazine reagents and liquid chromatography. *J Environ Monit* **3**(3):306-310.

Scott EE, He YA, Wester MR, White MA, Chin CC, Halpert JR, Johnson EF and Stout CD (2003) An open conformation of mammalian cytochrome P450 2B4 at 1.6-A resolution. *Proc Natl Acad Sci U S A* **100**(23):13196-13201.

Scott EE, White MA, He YA, Johnson EF, Stout CD and Halpert JR (2004) Structure of mammalian cytochrome P450 2B4 complexed with 4-(4-chlorophenyl)imidazole at 1.9-A resolution: insight into the range of P450 conformations and the coordination of redox partner binding. *J Biol Chem* **279**(26):27294-27301.

Sippl MJ (1993) Recognition of errors in three-dimensional structures of proteins. *Proteins* **17**(4):355-362.

Spatzenegger M, Liu H, Wang Q, Debarber A, Koop DR and Halpert JR (2003) Analysis of differential substrate selectivities of CYP2B6 and CYP2E1 by site-directed mutagenesis and molecular modeling. *J Pharmacol Exp Ther* **304**(1):477-487.

Thompson JD, Higgins DG and Gibson TJ (1994) CLUSTAL W: improving the sensitivity of progressive multiple sequence alignment through sequence weighting, position-specific gap penalties and weight matrix choice. *Nucleic Acids Res* **22**(22):4673-4680.

Truan G, Cullin C, Reisdorf P, Urban P and Pompon D (1993) Enhanced in vivo monooxygenase activities of mammalian P450s in engineered yeast cells producing high levels of NADPH-P450 reductase and human cytochrome b5. *Gene* **125**(1):49-55.

Tychopoulos M, Corcos L, Genne P, Beaune P and de Waziers I (2005) A virus-directed enzyme prodrug therapy (VDEPT) strategy for lung cancer using a CYP2B6/NADPH-cytochrome P450 reductase fusion protein. *Cancer Gene Ther* **12**(5):497-508.

Molecular Pharmacology Fast Forward. Published on January 22, 2008 as DOI: 10.1124/mol.107.042861
This article has not been copyedited and formatted. The final version may differ from this version.

Wallner B and Elofsson A (2003) Can correct protein models be identified? *Protein Sci* **12**(5):1073-1086.

Waxman DJ, Chen L, Hecht JE and Jounaidi Y (1999) Cytochrome P450-based cancer gene therapy: recent advances and future prospects. *Drug Metab Rev* **31**(2):503-522.

Yasukochi Y, Okita RT and Masters BS (1980) Comparison of the properties of detergent-solubilized NADPH-cytochrome P-450 reductases from pig liver and kidney. Immunochemical, kinetic, and reconstitutive properties. *Arch Biochem Biophys* **202**(2):491-498.

Zhao Y and Halpert JR (2006) Structure-function analysis of cytochromes P450 2B. *Biochim Biophys Acta*.

Zhao Y, White MA, Muralidhara BK, Sun L, Halpert JR and Stout CD (2006) Structure of microsomal cytochrome P450 2B4 complexed with the antifungal drug bifonazole: insight into P450 conformational plasticity and membrane interaction. *J Biol Chem* **281**(9):5973-5981.

Molecular Pharmacology Fast Forward. Published on January 22, 2008 as DOI: 10.1124/mol.107.042861
This article has not been copyedited and formatted. The final version may differ from this version.

Footnotes

a) **Financial supports**: This work was supported by the Region Bourgogne, the Ligue contre le Cancer and Oncodesign S.A. (Dijon, France).

b) **Reprint requests**: Isabelle de Waziers, INSERM UMR-S775, Faculté de Médecine, 45 rue des Saints Pères, 75270 Paris Cedex 06, France, e-mail: isabelle.waziers@univ-paris5.fr

Molecular Pharmacology Fast Forward. Published on January 22, 2008 as DOI: 10.1124/mol.107.042861
This article has not been copyedited and formatted. The final version may differ from this version.

Figures legends

Figure 1. **Dynamic properties of unliganded CYP2B6 (homology model, in red) and CYP2B4 (1SUO structure, in black).** Time dependence of root mean square deviations from the initial structure (RMSD, in Å) were calculated on backbone atoms by ProFit. For CYP2B4 dynamics (black), the initial structure was the 1SUO PDB structure equilibrated in the solvent box. For CYP2B6 (red), the initial structure was the best CYP2B6 model rebuilt from the CYP2B4 final structure derived after 2 ns of MD simulation. MD simulations were carried out in explicit solvent using the GROMACS v3.1.4 molecular dynamics simulation package. For details see the Materials and methods section.

Figure 2 : **Initial positioning of CPA in the active site of the CYP2B6 model:** The position of the CPI ring close to the heme iron in CYP2B4 (1SUO) was used to produce an initial positioning for CPA (S-enantiomer) in the CYP2B6 model. The metabolic (or inhibitory) atom sites of each molecule were superimposed as starting point before MD simulation (C and N atoms respectively, are indicated by a black arrow). Each structure (1SUO and CYP2B6 model) was equilibrated and relaxed in the same conditions by MD (2 ns), resulting in slightly different positions of the ligands relative to the heme.

Figure 3: **CYP2B6 active site showing residues potentially close to CPA (in blue) docked inside.** Some residues shown to be important for substrate metabolism and selected for mutagenesis studies (114, 367, 477, 478) are labeled and displayed as purple sticks. Heme is shown as orange sticks and CPA (S-enantiomer) as blue sticks. The contour of the active site computed by Voidoo is shown in grey mesh.

Molecular Pharmacology Fast Forward. Published on January 22, 2008 as DOI: 10.1124/mol.107.042861
This article has not been copyedited and formatted. The final version may differ from this version.

Figure 4: **CYP2B6 topology with the identified channels.** The channels have been identified by CAVER based on various structures produced during the 2 ns MD simulations. The channels are shown using the CAVER-generated van der Waals representation within the PYMOL graphical environment. Three major pathways to the buried active site were identified i) a class of channels (light orange, orange and red) close to the B-C loop on each side of helix B', ii) a channel between the E, F and I helices (blue), iii) and a channel along the I helix (purple). The protein is shown in a shaded gray cartoon representation. Alpha – helices are annotated with their corresponding letters. Panel A: top-view looking down on the heme cofactor from the distal side, Panel B: side-view looking down the I helix.

Figure 5: **CPA hydroxylase activity of double mutant V477W/I114V CYP2B6.** Enzymatic kinetic analysis of cyclophosphamide 4-hydroxylation was performed using microsomes from yeasts expressing the double mutant V477W/I114V CYP2B6 according to the Materials and methods section. Kinetic constants of CPA hydroxylase were determined by a non-linear regression with fifteen substrate concentrations (0.05 to 25 mM) Km and Vmax were calculated using GraphPad Prism Software. Data shown were based on duplicate determinations for each data point.

Figure 6: **Geometry of the active site of wt CYP2B6 (A) and CYP2B6 V477W/I114V (B) (side and top views). A:** Some residues shown to be important for substrate metabolism and selected for mutagenesis studies (114, 367, 477, 478) are labeled and displayed as purple sticks. Heme is shown as orange sticks and CPA (S-enantiomer) as blue sticks. The contour of the active site computed by Voidoo is shown in grey mesh. **B.** Changes in the orientation of the active site are shown in the mutant model. Mutated residues 114 and 477 are labeled and displayed as magenta sticks. Heme is shown as orange sticks and CPA as blue sticks. The

Molecular Pharmacology Fast Forward. Published on January 22, 2008 as DOI: 10.1124/mol.107.042861
This article has not been copyedited and formatted. The final version may differ from this version.

contour of the active site computed by Voidoo is shown in grey mesh. After double mutation, the active site is flattened by the presence of a tryptophan side chain, which causes steric displacement at the top, and widened at the basis of the site in the vicinity of the heme.

Figure 7: **Dynamic behavior of CPA in the active site of wt CYP2B6 vs CYP2B6 V477W/I114V**: RMSD fluctuations of CPA (S-enantiomer) during 2 ns of MD simulation calculated by the g_rms function of GROMACS and, showing the deviation from the average position of the substrate as a function of time. Amplitudes of fluctuations are attenuated in the mutant model (maximum amplitude observed is represented in the margin by red and black arrows for the wt and double mutant, respectively). All structures are fitted pairwise by g_rms with starting structure taken as reference. Note that the RMSD levels reached at equilibrium (1Å and 1.2Å for wt and double mutant, respectively) are different and cannot be compared as they are dependent upon the initial positioning.

Figure 8: MTS cytotoxicity assays for A-253 cells. CPA-induced cytotoxicity assays were performed in cells infected with different adenoviral vectors expressing LacZ, CYP2B6 (2B6), double mutant V477W/I114V CYP2B6 (2B6 double mutant) or the human reductase (Red). Cytotoxicity was assayed using a MTS colorimetric test, which measures the dehydrogenase activity in the metabolically active mitochondria of viable cells as described in the Materials and Methods section. Cell viability is expressed as the percentage of viable cells compared to those infected with control vector (Ad-LacZ) treated at identical CPA concentrations and compared to untreated cells for each infection. The assays were repeated four times in triplicate and the bars represent standard deviation.

Molecular Pharmacology Fast Forward. Published on January 22, 2008 as DOI: 10.1124/mol.107.042861
This article has not been copyedited and formatted. The final version may differ from this version.

Figure 9. Active site in the V477Y mutant, side and top views. The black arrow indicates potential hydrogen bonding between the OH group of the Tyr477 and the carboxylate group of Glu 301. Side chains and heme are displayed as green sticks.

Molecular Pharmacology Fast Forward. Published on January 22, 2008 as DOI: 10.1124/mol.107.042861
This article has not been copyedited and formatted. The final version may differ from this version.


```
CYP2B11   MELSVLLLLA LLTGLLLLMA RGHPKAYGHL PPGPRPLPIL GNFLQMDRKG LLKSFLRLQE   60
CYP2B5    MEFSLLLLLA FLAGLLLLLF RGHPKAHGRL PPGPPPLPVL GNLLQMDRKG LLRSFLRLRE   60
CYP2B2    MEPSILLLLA LLVGFLLLLV RGHPKSRGNF PPGPRPLPLL GNLLQLDRGG LLNSFMQLRE   60
CYP2B1    MEPTILLLLA LLVGFLLLLV RGHPKSRGNF PPGPRPLPLL GNLLQLDRGG LLNSFMQLRE   60
CYP2B6    MELSVLLFLA LLTGLLLLLV QRHPNTHDRL PPGPRPLPLL GNLLQMDRRG LLKSFLRFRE   60
CYP2B4    MEFSLLLLLA FLAGLLLLLF RGHPKAHGRL PPGPSPLPVL GNLLQMDRKG LLRSFLRLRE   60
                                                        A'          A
                                                          SRS1
CYP2B11   KYGDVFTVYL GPRRTVMLCG IDAIREALVD NAEAFSGRGK IAVVEPVFQG YGVVFANGER  120
CYP2B5    KYGDVFTVYL GSRPVVVLCG TDAIREALVD QAEAFSGRGK IAVVDPIFQG YGVFFANGEH  120
CYP2B2    KYGDVFTVHL GPRPVVMLCG TDTIKEALVG QAEDFSGRGT IAVIEPIFKE YGVIFANGER  120
CYP2B1    KYGDVFTVHL GPRPVVMLCG TDTIKEALVG QAEDFSGRGT IAVIEPIFKE YGVIFANGER  120
CYP2B6    KYGDVFTVHL GPRPVVMLCG VEAIREALVD KAEAFSGRGK IAMVDPFFRG YGVIFANGNR  120
CYP2B4    KYGDVFTVYL GSRPVVVLCG TDAIREALVD QAEAFSGRGK IAVVDPIFQG YGVIFANGER  120
                β1-1       β1-2        B            β1-5       B'            C

CYP2B11   WKTLRRFSLA TMRDFGMGKR SVEERIQEEA QCLVEELRKT EGVLQDPTFF FHSMTANIIC  180
CYP2B5    WRALRRFSLA TMRDFGMGKR SVEERIQEEA RCLVEELRKS KGALLDNTLL FHSVTSNIIC  180
CYP2B2    WKALRRFSLA TMRDFGMGKR SVEERIQEEA QCLVEELRKS QGAPLDPTFL FQCITANIIC  180
CYP2B1    WKALRRFSLA TMRDFGMGKR SVEERIQEEA QCLVEELRKS QGAPLDPTFL FQCITANIIC  180
CYP2B6    WKVLRRFSVT TMRDFGMGKR SVEERIQEEA QCLIEELRKS KGALMDPTFL FQSITANIIC  180
CYP2B4    WRALRRFSLA TMRDFGMGKR SVEERIQEEA RCLVEELRKS KGALLDNTLL FHSITSNIIC  180
                                        D                β3-1          E
                                   SRS2                                 SRS3
CYP2B11   SIVFGKRFGY KDPEFLRLMN LFYVSFALIS SFSSQMFELF HSFLKYFPGT HRQVYNNLQE  240
CYP2B5    SIVFGKRFDY KDPVFLRLLD LFFQSFSLIS SFSSQVFELF PGFLKHFPGT HRQIYRNLQE  240
CYP2B2    SIVFGERFDY TDRQFLRLLE LFYRTFSLLS SFSSQVFEFF SGFLKYFPGA HRQISKNLQE  240
CYP2B1    SIVFGERFDY TDRQFLRLLE LFYRTFSLLS SFSSQVFEFF SGFLKYFPGA HRQISKNLQE  240
CYP2B6    SIVFGKRFHY QDQEFLKMLN LFYQTFSLIS SVFGQLFELF SGFLKYFPGA HRQVYKNLQE  240
CYP2B4    SIVFGKRFDY KDPVFLRLLD LFFQSFSLIS SFSSQVFELF SGFLKHFPGT HRQIYRNLQE  240
                            F                F'       G'            G
                                                                   SRS4
CYP2B11   IKAFIARMVE KHRETLDPSA PRDFIDAYLI RMDKEKAEPS SEFHHRNLID TALSLFFAGT  300
CYP2B5    INTFIGQTVE KHRATLDPSN PRDFIDVYLL RMEKDKSDPS SEFHHRNLIL TVLTLFFAGT  300
CYP2B2    ILDYIGHIVE KHRATLDPSA PRDFIDTYLL RMEKEKSNHH TEFHHENLMI SLLSLFFAGT  300
CYP2B1    ILDYIGHIVE KHRATLDPSA PRDFIDTYLL RMEKEKSNHH TEFHHENLMI SLLSLFFAGT  300
CYP2B6    INAYIGHSVE KHRETLDPSA PKDLIDTYLL HMEKEKSNAH SEFSHQNLNL NTLSLFFAGT  300
CYP2B4    INTFIGQSVE KHRATLDPSN PRDFIDVYLL RMEKDKSDPS SEFHHQNLIL TVLSLFFAGT  300
                                        H                            I

CYP2B11   ETTSTTLRYG FLLMLKYPHI AERIYKEIDQ VIGPHRLPSL DDRAKMPYTD AVIHEIQRFG  360
CYP2B5    ETTSTTLRYG FLLMLKYPHV TERVQKEIEQ VIGSHRPPAL DDRAKMPYTD AVIHEIQRLG  360
CYP2B2    ETGSTTLRYG FLLMLKYPHV TEKVQKEIDQ VIGSHRPPSL DDRTKMPYTD AVIHEIQRFA  360
CYP2B1    ETSSTTLRYG FLLMLKYPHV AEKVQKEIDQ VIGSHRLPTL DDRSKMPYTD AVIHEIQRFS  360
CYP2B6    ETTSTTLRYG FLLMLKYPHV AERVYREIEQ VIGPHRPPEL HDRAKMPYTE AVIYEIQRFS  360
CYP2B4    ETTSTTLRYG FLLMLKYPHV TERVQKEIEQ VIGSHRPPAL DDRAKMPYTD AVIHEIQRLG  360
                                   J                    J'         K
          SRS5
CYP2B11   DLLPIGVPHM VTKDICFRGY IIPKGTEVFP ILHSALNDPH YFEKPDVFNP DHFLDANGAL  420
CYP2B5    DLVPFGAPHM VTKDTQFRGY VIPKNTEVFP VLSSALHDPR YFETPNTFNP GHFLDADGAL  420
CYP2B2    DLAPIGLPHR VTKDTMFRGY LLPKNTEVYP ILSSALHDPQ YFDHPDTFNP EHFLDADGTL  420
CYP2B1    DLVPIGVPHR VTKDTMFRGY LLPKNTEVYP ILSSALHDPQ YFDHPDSFNP EHFLDANGAL  420
CYP2B6    DLLPMGVPHI VTQHTSFRGY IIPKDTEVFL ILSTALHDPH YFEKPDAFNP DHFLDANGAL  420
CYP2B4    DLIPFGVPHT VTKDTQFRGY VIPKNTEVFP VLSSALHDPR YFETPNTFNP GHFLDANGAL  420
                β1-4       β2-1    β2-2    β1-3      K'                K''
                                                                   SRS6
CYP2B11   KKNEAFIPFS IGKRICLGEG IARMELFLFF TTILQNFSVA SPMAPEDIDL TPQEIGVGKL  480
CYP2B5    KRNEGFMPFS LGKRICLGEG IARTELFLFF TTILQNFSIA SPVPPEDIDL TPRESGVGNV  480
CYP2B2    KKSEAFMPFS TGKRICLGEG IARNELFLFF TTILQNFSVS SHLAPKDIDL TPKESGIAKI  480
CYP2B1    KKSEAFMPFS TGKRICLGEG IARNELFLFF TTILQNFSVS SHLAPKDIDL TPKESGIGKI  480
CYP2B6    KKTEAFIPFS LGKRICLGEG IARAELFLFF TTILQNFSMA SPVAPEDIDL TPQECGVGKI  480
CYP2B4    KRNEGFMPFS LGKRICLGEG IARTELFLFF TTILQNFSIA SPVPPEDIDL TPRESGVGNV  480
                     K'''            L            β3-3       L'        β4-1 β4-2

CYP2B11   PPVYQISFLS RGGC 494
CYP2B5    PPSYQIRFLA R--- 491
CYP2B2    PPTYQICFSA R--- 491
CYP2B1    PPTYQICFSA R--- 491
CYP2B6    PPTYQIRFLP R--- 491
CYP2B4    PPSYQIRFLA R--- 491
                β3-2
```

Table 1. **Sequence alignment of CYP2B11, CYP2B6, CYP2B4, CYP2B5, CYP2B2 and CYP2B1** using clustalw software (http://www.ebi.ac.uk/clustalw). Substrate recognition sites (SRS) are indicated along the sequence. Helices are underlined in red and sheets in orange. Mutations in the active site are written in red, canine mutations in magenta and genetic polymorphism in blue. The first 27 N-terminal residues of CYP2B4 (in green) were not present in the crystallized CYP2B4 and were deleted in the CYP2B6 model.

Molecular Pharmacology Fast Forward. Published on January 22, 2008 as DOI: 10.1124/mol.107.042861
This article has not been copyedited and formatted. The final version may differ from this version.

Mutation	CYP content	Vmax		Km		Vmax/Km	
	pmol/mg	min^{-1}	% of wt	mM	% of wt		% of wt
CYP2B6wt	112	62.5	100	4.9	100	12.8	100
Mutations in active site							
I114V	93	65.2	104	2.3	47	28.4	221
V367L	50	90.3	144	8.8	181	10.2	80
V367F	29	26.8	43	12.9	264	2.1	16
V367S	54	5.2	8	NQ			
V367T	30	24.2	39	6.4	131	3.8	30
V367H	17	1.5	2	NQ			
V477S	82	N.D	-	NQ			
V477T	76	37.2	59	8.9	182	4.2	33
V477Y	70	28.6	46	5.9	121	4.9	38
V477N	126	N.D	-	NQ			
V477D	53	2.5	4	NQ			
V477E	72	1.8	3	NQ			
V477I	53	77.4	124	3.2	66	24.2	189
V477F	104	81.1	130	3.3	68	24.5	191
V477W	203	99.9	160	2.8	57	35.7	278
G478A	75	28	45	6.3	129	4.4	35
G478V	81	36.3	58	2.6	53	14.2	110
G478S	139	7.5	12	NQ			
G478E	48	5.4	9	NQ			
"canine mutations"							
F107V	180	95.9	153	6.5	133	14.8	115
L199M	70	125.2	200	4.8	98	26.3	205
S207A	90	69.9	112	5.5	113	12.7	99
K236N	40	47	75	56.2	1153	0.8	7
M365I	340	12.9	21	3.8	77	3.4	27
C475I	190	1.7	3	4.7	96	0.4	3
Double mutant							
I114V +V477W	120	58.5	94	1.1	23	52.7	411

Table 2. CYP content and enzyme kinetic analysis of CPA 4-hydroxylation in yeast microsomes expressing wild type CYP2B6 and site-directed mutants. CYP content was spectrally determined (Schoene et al., 1972). Data were calculated using GraphPad Prism Software. Fifteen substrate concentrations from 0-25 mM were used for enzymatic analysis. Vmax values for CPA hydroxylase were expressed as moles of product formed per minute per mole of CYP included in the reaction. Km values in mM were obtained after kinetic analysis derived from nonlinear regression. ND: not detectable, NQ: not quantifiable.

Molecular Pharmacology Fast Forward. Published on January 22, 2008 as DOI: 10.1124/mol.107.042861
This article has not been copyedited and formatted. The final version may differ from this version.

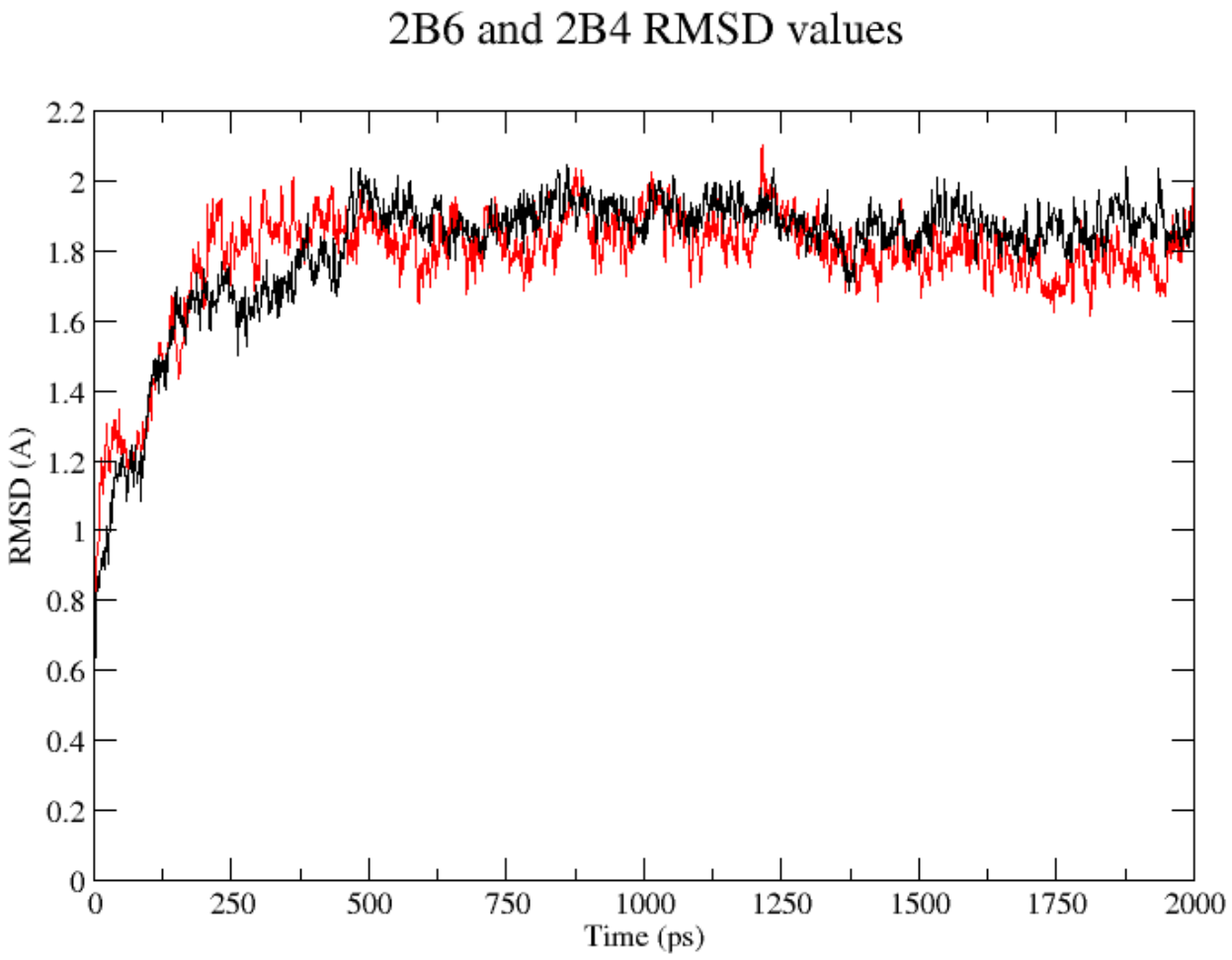

Figure 1

Molecular Pharmacology Fast Forward. Published on January 22, 2008 as DOI: 10.1124/mol.107.042861
This article has not been copyedited and formatted. The final version may differ from this version.

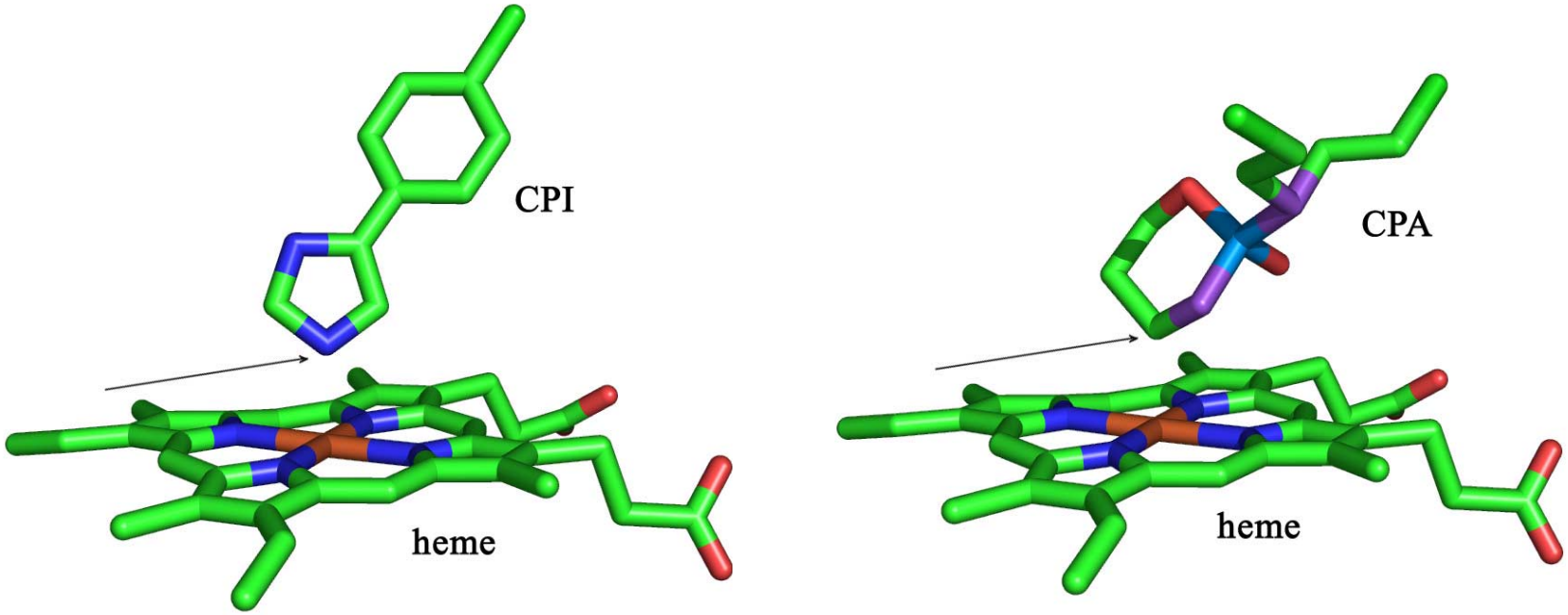

Figure 2

Molecular Pharmacology Fast Forward. Published on January 22, 2008 as DOI: 10.1124/mol.107.042861
This article has not been copyedited and formatted. The final version may differ from this version.

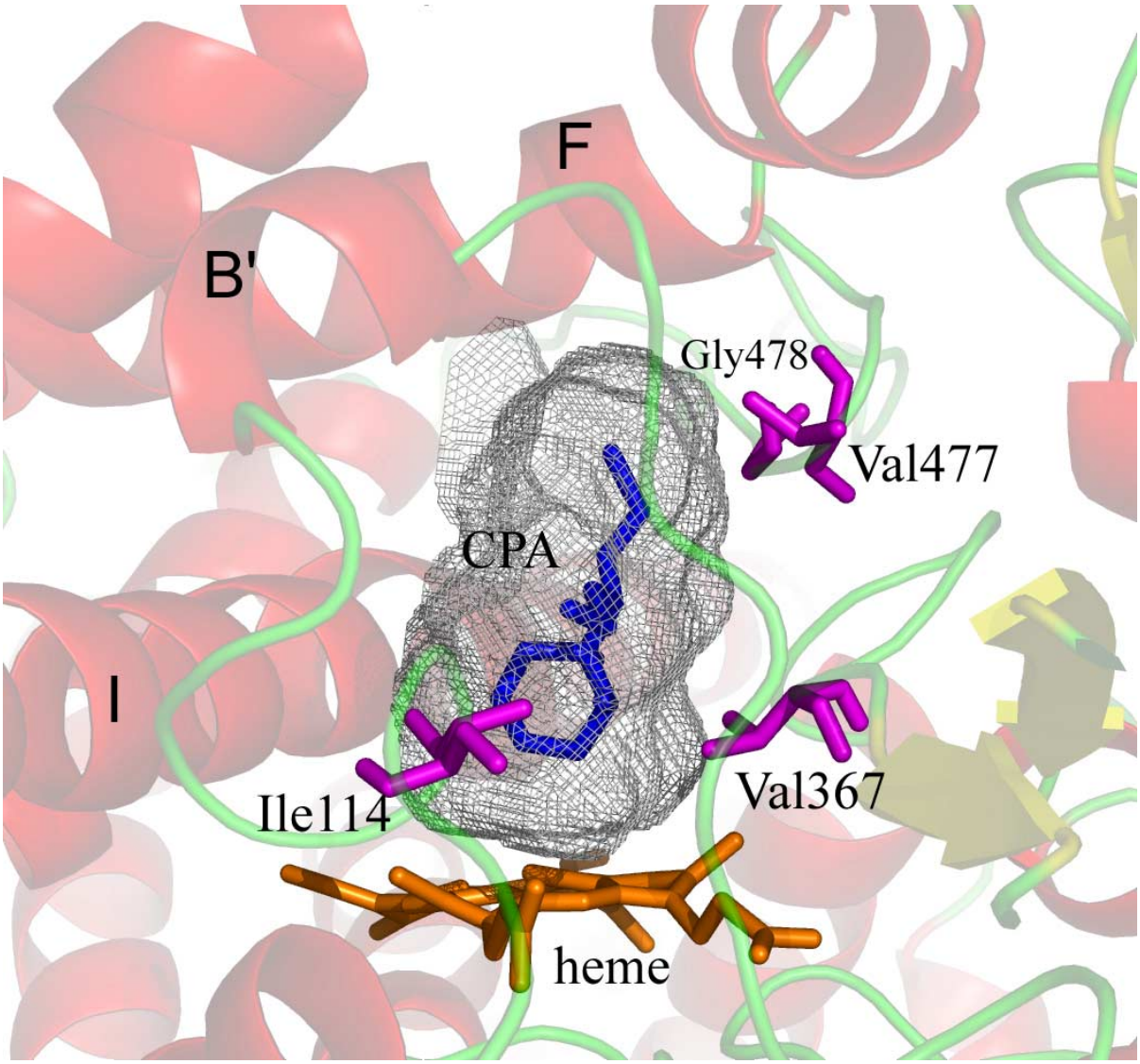

Figure 3

Molecular Pharmacology Fast Forward. Published on January 22, 2008 as DOI: 10.1124/mol.107.042861
This article has not been copyedited and formatted. The final version may differ from this version.

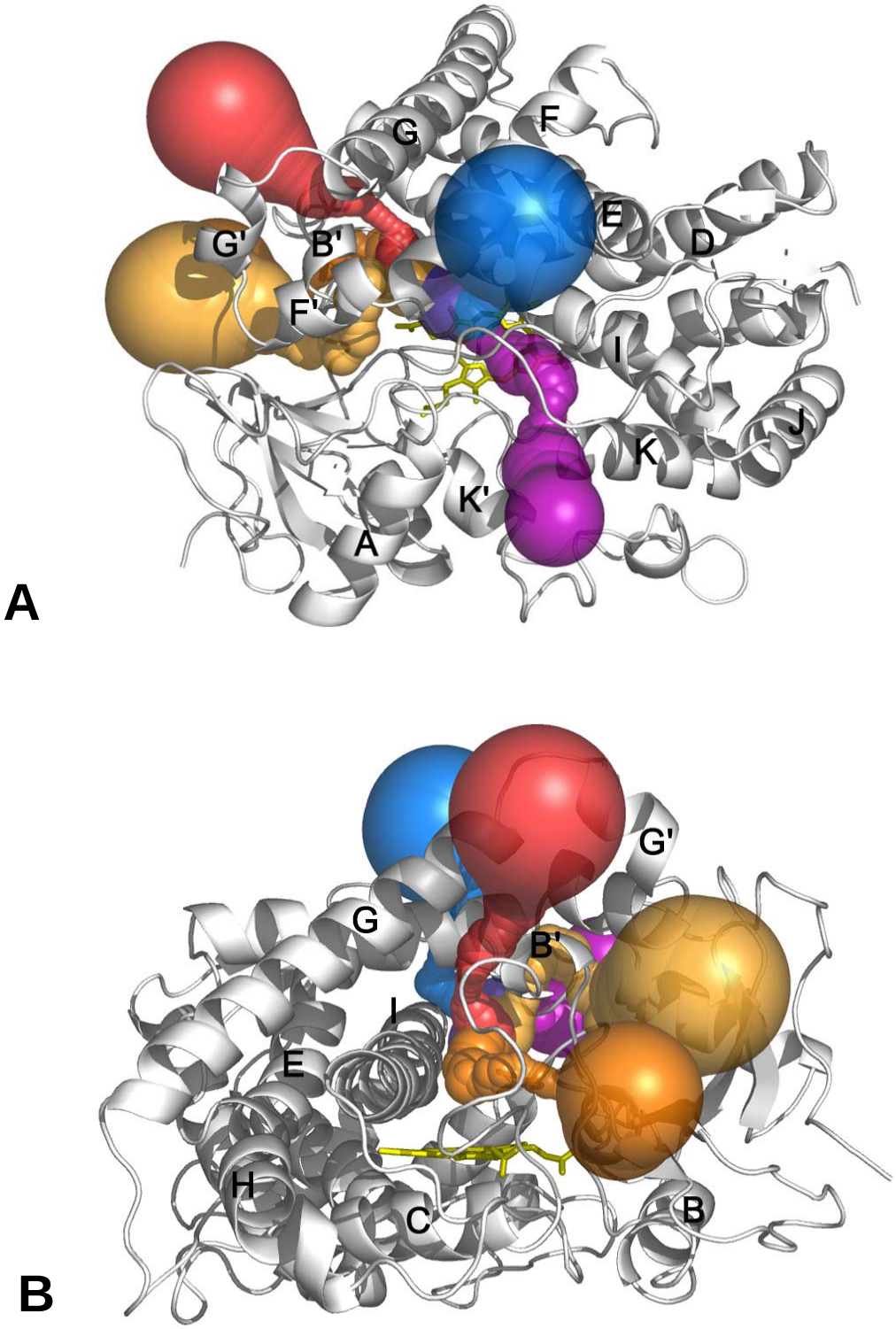

Figure 4

Molecular Pharmacology Fast Forward. Published on January 22, 2008 as DOI: 10.1124/mol.107.042861
This article has not been copyedited and formatted. The final version may differ from this version.

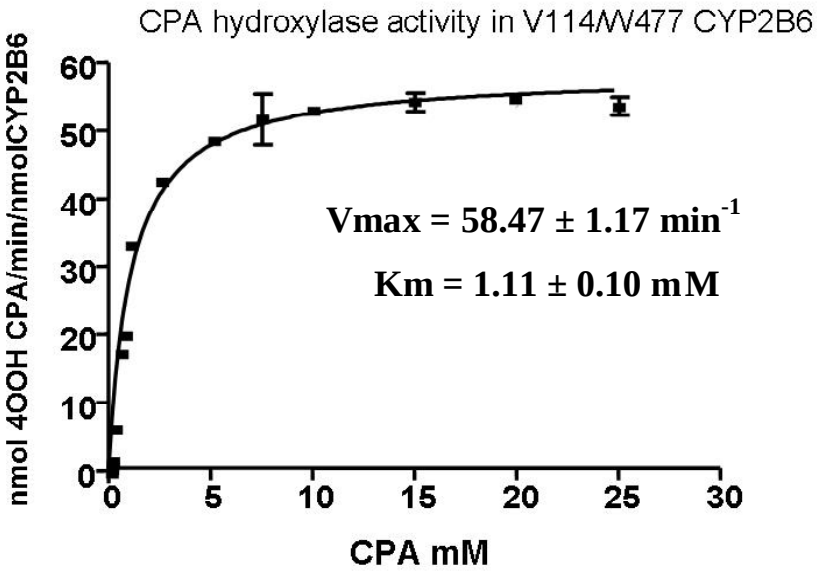

Figure 5.

Molecular Pharmacology Fast Forward. Published on January 22, 2008 as DOI: 10.1124/mol.107.042861
This article has not been copyedited and formatted. The final version may differ from this version.

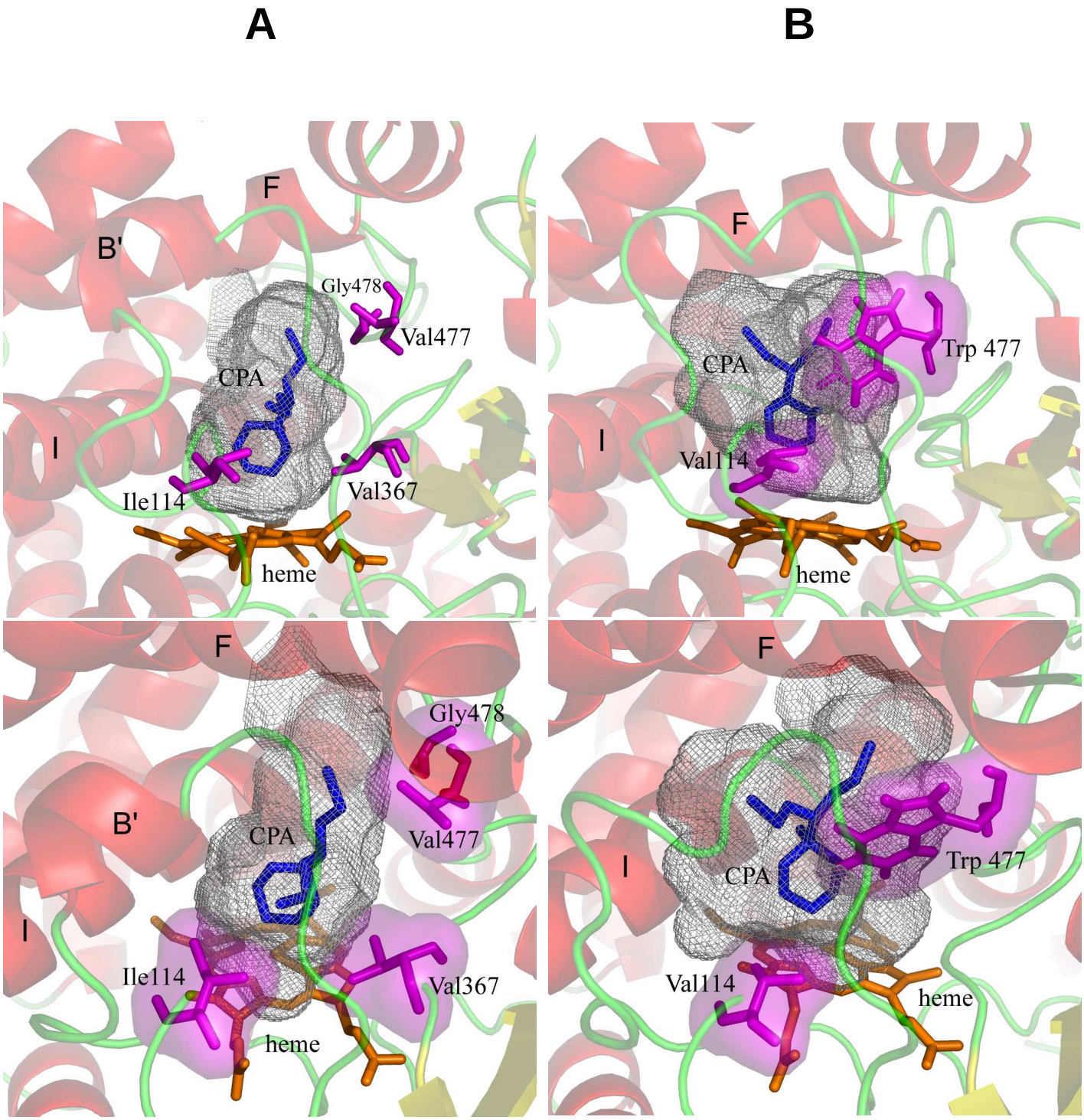

Figure 6

Molecular Pharmacology Fast Forward. Published on January 22, 2008 as DOI: 10.1124/mol.107.042861
This article has not been copyedited and formatted. The final version may differ from this version.

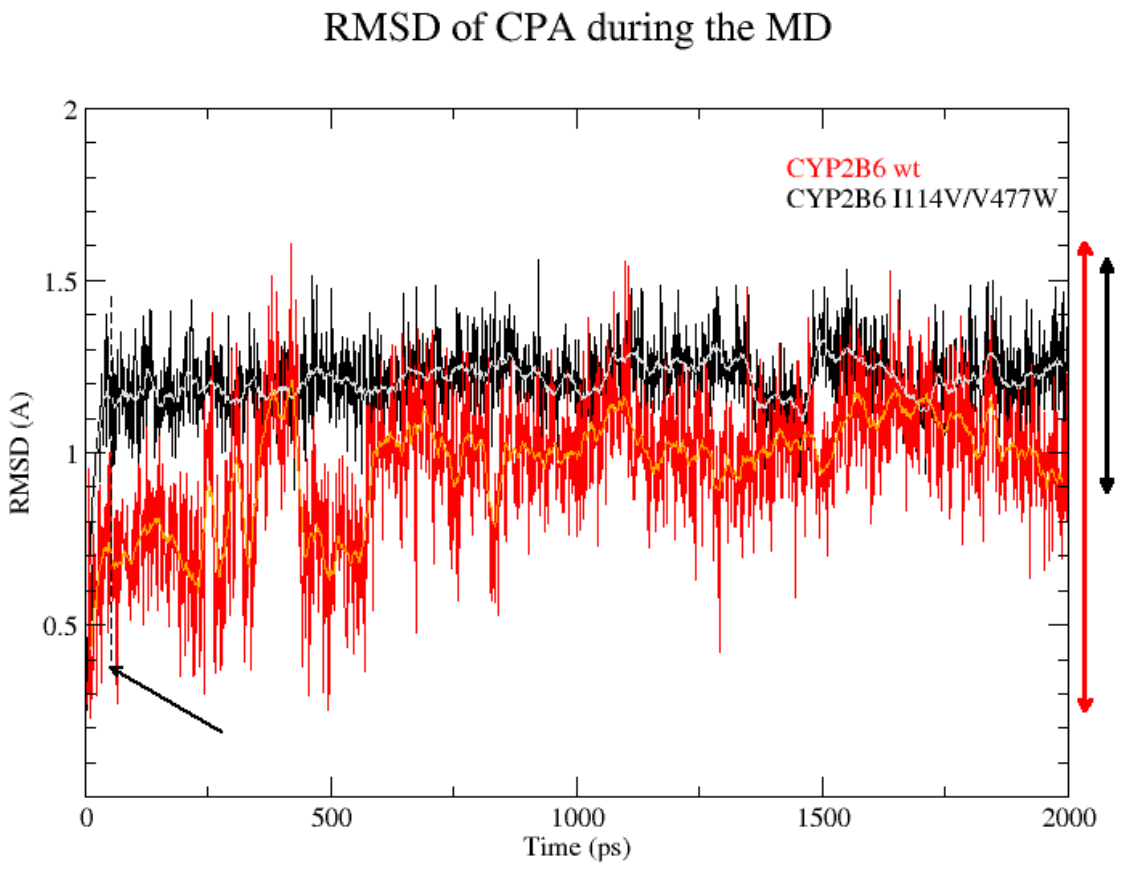

Figure 7

Molecular Pharmacology Fast Forward. Published on January 22, 2008 as DOI: 10.1124/mol.107.042861
This article has not been copyedited and formatted. The final version may differ from this version.

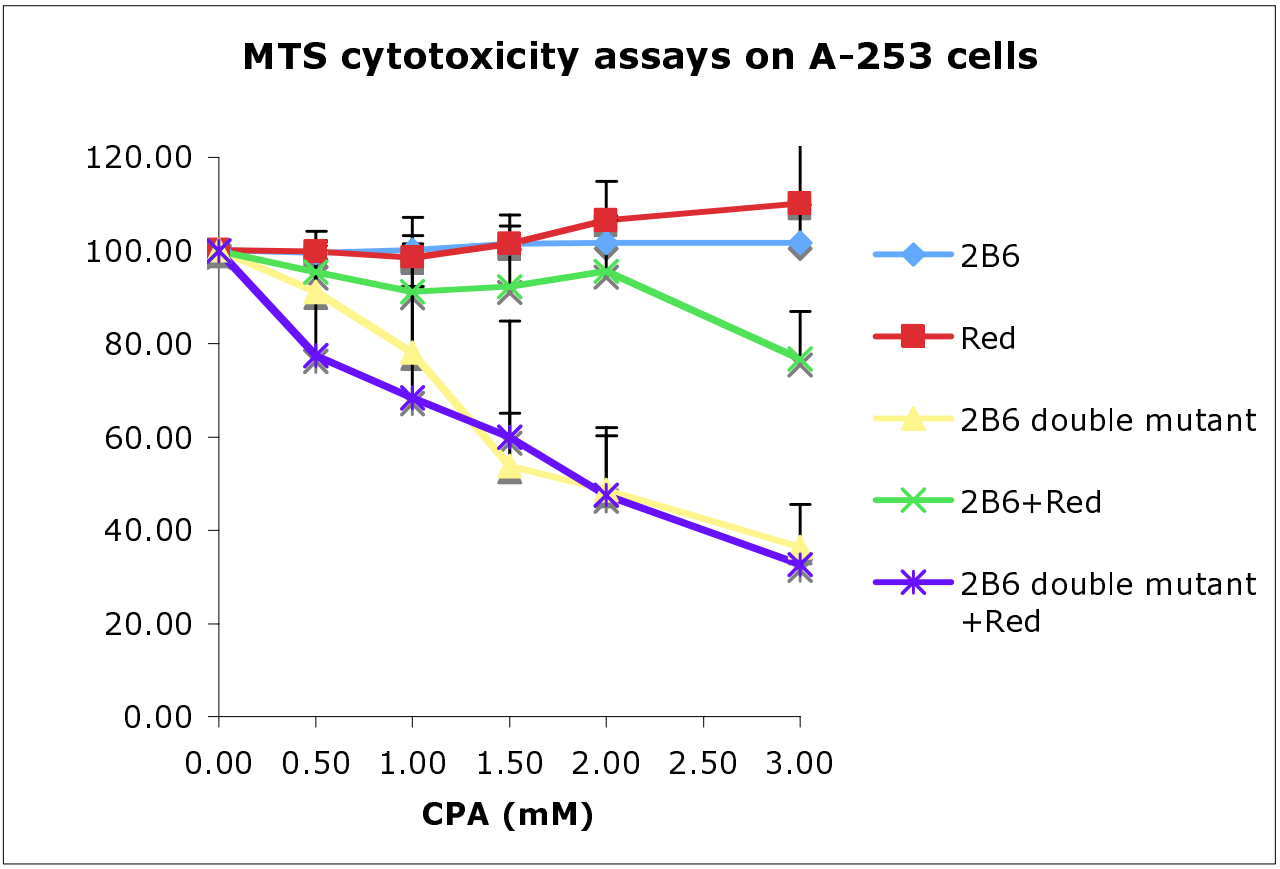

Figure 8

Molecular Pharmacology Fast Forward. Published on January 22, 2008 as DOI: 10.1124/mol.107.042861
This article has not been copyedited and formatted. The final version may differ from this version.

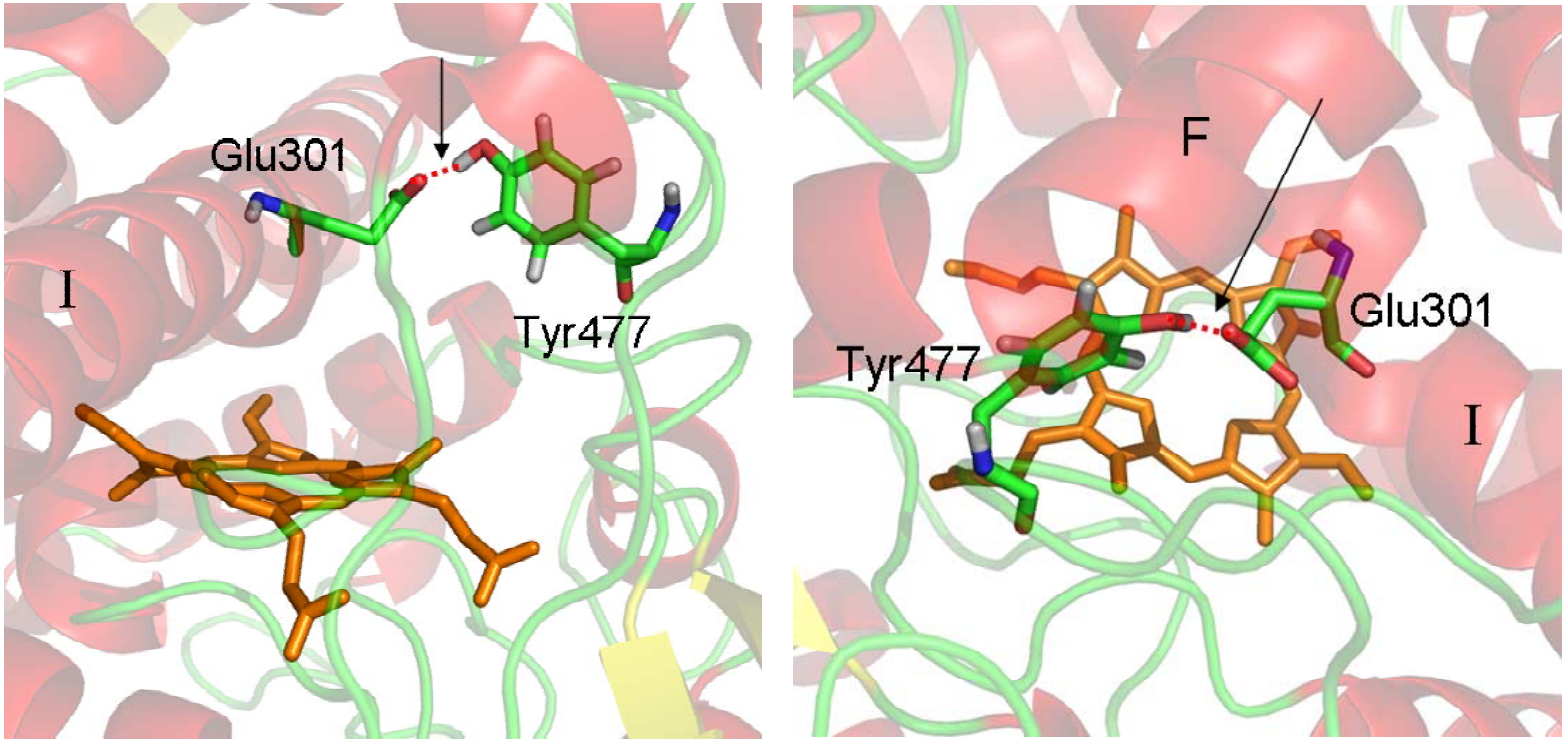

Figure 9